TÜBİTAK

Turkish Journal of Earth Sciences

http://journals.tubitak.gov.tr/earth/

Research Article

Turkish J Earth Sci
(2022) 31: 597-621

doi:10.55730/1300-0985.1822

Vertical variations of minerals in clayey sedimentary rocks in the cores of two-deep exploration wells from the Kozlu coalfield (Zonguldak, NW Türkiye), with emphasis on tonstein (schieferton) formation

Ali İhsan KARAYİĞİT[1,*], Emine CİCİOĞLU SÜTCÜ[2], Abidin TEMEL[1], Mustafa Niyazi GÜNDOĞDU[1]

[1]Hacettepe University, Department of Geological Engineering, Ankara, Turkey

[2]MTA, Mineral Analysis and Technology Department, Ankara, Turkey

Received: 15.05.2022 • **Accepted/Published Online:** 07.10.2022 • **Final Version:** 16.11.2022

Abstract: The majority of Turkish bituminous coal resources are located in the Zonguldak Basin. The Carboniferous coal seams in the Alacaağzı, Kozlu, and Karadon formations have received interest. However, the detailed mineralogical compositions of clayey sedimentary rocks in coal-bearing sequences in the basin have been limited. This study aims to investigate vertical variations of mineralogical compositions of Carboniferous and Early Cretaceous clayey sedimentary rocks cored in the two-deep exploration wells (K20/K and K20/H) from the Kozlu coalfield using XRD and SEM-EDX analyses data. In addition, a special interest is also given to tonstein layers identified within the Kozlu and Karadon formations. The XRD analyses revealed that the quartz and clay minerals are the main components, and the latter is generally the dominant phase in all studied formations. Besides, clay fraction minerals (chlorite, illite/mica, and kaolinite) are common, while illite/smectite mixed-layer clay mineral is only identified in the two samples. The tonstein samples display similar mineralogical compositions to other samples, while several accessory minerals (e.g., apatite, baddeleyite, monazite, and zircon) are also present. Furthermore, calcite, dolomite, and hematite are mainly observed from the Early Cretaceous samples of the Zonguldak Formation. The vertical distributions of quartz and clay fraction minerals are variable throughout the studied two exploration wells. The vertical variations of clay fraction mineral illite/mica could be mainly related to changes in clastic influx from the basement, while kaolinite seems to be controlled by synchronous volcanic inputs during the Carboniferous. This could also be evident by the predominance of kaolinite and associated volcanogenic mineral grains in tonstein samples. The common presence of carbonate minerals in the Zonguldak Formation is clearly related to shallow marine depositional conditions, while hematite in the reddish mudstone and claystone samples of this formation could be related to short-term terrestrization during the Cretaceous or afterwards.

Keywords: Zonguldak basin, mineralogy, kaolinite, tonstein, zircon, baddeleyite

1. Introduction

The most important bituminous coal resources and underground coal-production areas in the Zonguldak Basin within İstanbul Zone are located in the Armutçuk, Kozlu, Üzülmez, Gelik, and Amasra coalfields (Figure 1), where the coal resources are around 1.5 Gt (Karayiğit et al., 1998, Karayiğit et al., 2018a, 2018b).

The geological, sedimentological, palaeopalynological, mineralogical, petrographical, geochemical, and porosity features of Carboniferous (Namurian (Serpukhovian-Bashkirian), Westphalian A (Langsettian) and BCD (Duckmantian-Asturian) seams in the Zonguldak Basin and their coal-bed methane (CBM) potential were widely investigated (e.g., Ağralı, 1969; Kerey, 1985; Karayiğit, 1991, 1992; Akgün and Akyol, 1992; Canca, 1994; Yilmaz et al., 1997; Karayiğit et al., 1998; Tüysüz, 1999; Burger et al., 2000; Karacan and Okandan, 2000; Yalçın et al., 2002; Cleal and van Waveren, 2012; Okay and Nikishin, 2015; Tüysüz et al., 2016; Karayiğit et al., 2018a, 2018b; Opluštil et al., 2018). During 1990s, coal geology, palaeopalynology, and CBM studies were conducted from Carboniferous coal seams cored in the deep exploration wells by various researchers (Figure 1) (Gürdal and Yalçın, 2000; Yürüm et al., 2001; Yalçın et al., 2002; Karayiğit et al., 2018a). The results of these studies show that the coal seams are mainly gas-prone and have CBM generation potential. Furthermore, their porosity features are controlled by a combination of maceral and mineralogical features. The mineralogical compositions of seams are also controlled by the redox conditions within palaeomires and synchronous volcanic inputs during peat accumulation and penetration of hydrothermal solutions, which presumably originated

* Correspondence: aik@hacettepe.edu.tr

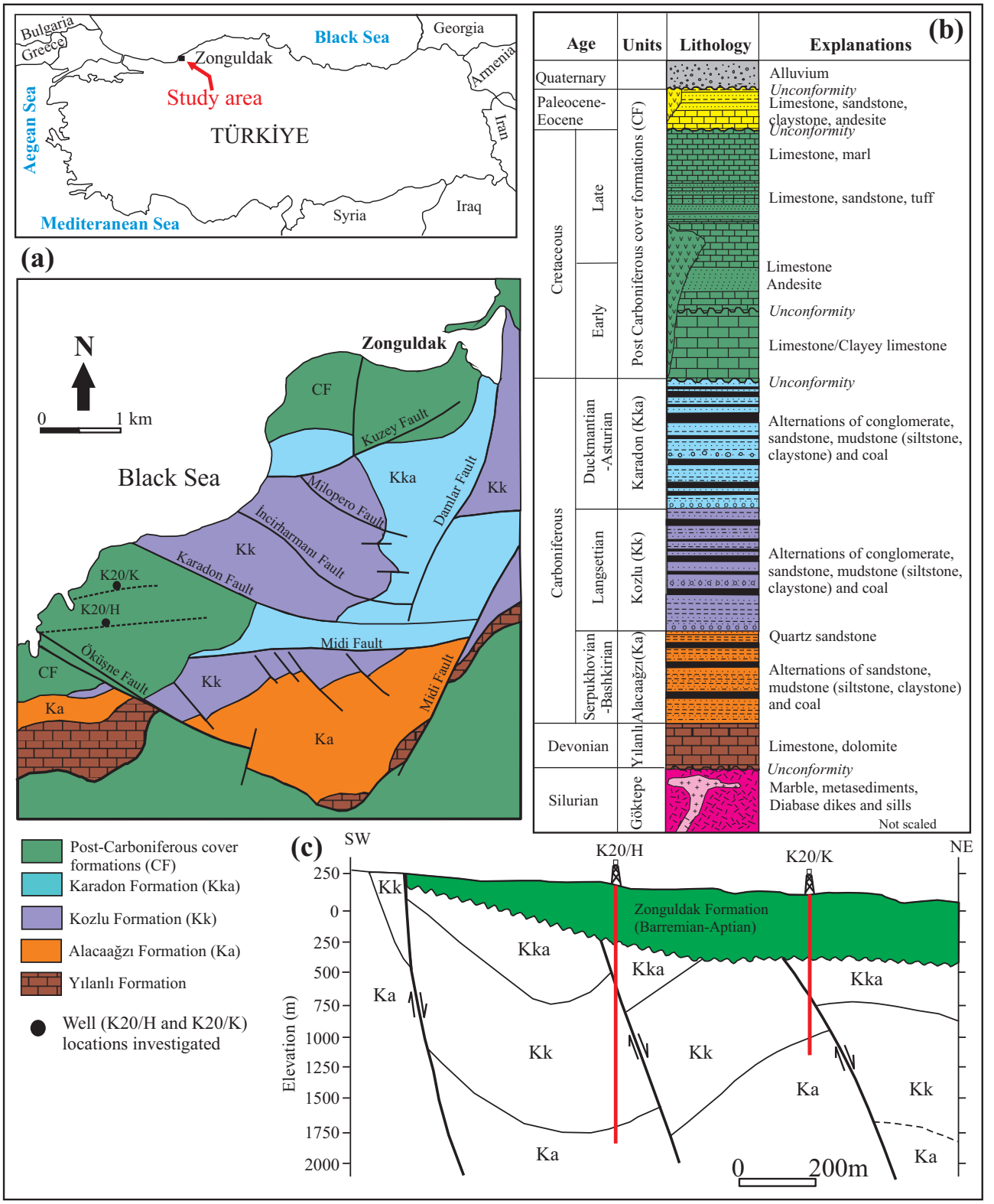

Figure 1. (a) The location and geological maps and (b) stratigraphic column of the Zonguldak Basin, and (c) the cross-section between studied wells (modified and simplified from Canca, 1994; Karayiğit, 2018a; Küskü et al., 1997; Yalçın et al., 2002).

from Cretaceous dykes in the basin during postcoalification (Karayiğit et al., 2018b).

The clay mineralogy of the coal seams in the coalfields from the Zonguldak Basin is quite interesting. For instance, individual vermicules of syngenetic kaolinite grains and kaolinitic matrices aggregated with apatite, biotite, chlorite, feldspars, quartz, and zircon grains are common, and similar assemblages and individual kaolinite grains were also identified from tonstein layers, also locally known as "*schieferton-like partings*" (Burger et al., 2000; Karayiğit et al., 2018a, 2018b). Furthermore, in some coal seams, illitic clay matrices and cleat/fracture kaolinite and chlorite infillings along with silica, carbonate, and sulphate minerals are also observed in the coal seams (Karayiğit et al., 2018a, 2018b). All these imply that kaolinite and chlorite in coal seams are mostly of syngenetic origin and by-products of alteration of volcanongenic materials and illite/mica is mainly related to clastic influx into palaeomire, while, to a lesser extent, kaolinite and chlorite are of epigenetic origin. Although mineralogical compositions of coal seams in the basin have been studied in detail previously, there is no comprehensive published study about the mineralogy of clayey sedimentary rocks in the coal-bearing Carboniferous sequences. Therefore, this study targeted the determination of mineralogical compositions of the clayey sedimentary rocks alternated with the coal layers cored by two-deep exploration wells, namely K20/H with 2002.20m and K20/K with 1251.61 m depth from the surface, and the specific goal was to identify the vertical variations of mineral compositions, and to ascertain controlling factors of mineralogical variations. In addition, special interest is also given to a few tonstein (schieferton) layers.

2. Geological background

The basement rocks of the basin consist of Silurian meta-sediments, and Devonian aged volcanic rocks and marine carbonates (Dean et al., 2000; Yalçın et al., 2002). In the study area, the coal-bearing Carboniferous-aged sequence is represented by Alacaağzı (Serpukhovian-Bashkirian), Kozlu (Langsettian), and Karadon (Duckmantian-Asturian) formations (Figure 1) (Ağralı, 1969; Kerey, 1985; Canca, 1994; Akgün and Akyol, 1992; Yalçın et al., 2002; Opluštil et al., 2018). The Alacaağzı formation is generally represented by black-colored claystones, which are generally rich in organic matter (Kerey, 1985; Yalçın et al., 2002; Opluštil et al., 2018). There are three cross-bedded sandstone layers with a 2–10 m thickness at the lower part of the formation, and the thin sandstone layers alternate with the claystones at the upper part of the formation. In addition, two coal seams within the Alacaağzı Formation were cored in the K20/H and nine coal seams in the K20/K well, and the thickness of these seams ranged from 5 to 65 cm (Karayiğit et al., 2018a). Previous sedimentological studies show that the Alacaağzı Formation was deposited in small, shallow lakes in the upper delta plain environment (Kerey, 1985; Yalçın et al., 2002; Opluštil et al., 2018). This formation is conformably overlain by the Kozlu Formation, which is composed of alteration of coal seams, claystone, siltstone, mudstone, sandstone, and conglomerate, which were deposited under delta and lacustrine environments (Figure 1). The sedimentological features imply that the Kozlu formation is composed of cyclical sequences deposited in braided/meandering rivers and lacustrine environments (Kerey, 1985; Yalçın et al., 2002; Opluštil et al., 2018). The most distinct feature of the Kozlu Formation is that it hosts a total of twenty-eight workable coal seams, which support the coal production in the Zonguldak Basin (Karayiğit et al., 1998; Karayiğit et al., 2018b). The Karadon formation of Langsettian age conformably overlies the Kozlu Formation and it has similar lithological units as the Kozlu Formation (Figures 1a and 1b). However, the thickness and extent of the coal seams in the Karadon Formation are not as significant as in the Kozlu Formation. In the Karadon Formation, four economic coal seams occur (Karayiğit et al., 1998; Karayiğit et al., 2018a, 2018b). Besides these seams in the Kozlu and Karadon formations, tonstein (schieferton) layers were also identified in these formations (Burger et al., 2000; Karayiğit et al., 1998; Karayiğit et al., 2018a). As a result of the Hercynian and Alpine orogenies, the coal-bearing Carboniferous sequences in the basin were exposed to intense folding and faulting (Figures 1a and 1c). Therefore, the thickness and lithology of the formations cut in the two-deep exploration wells show some differences, even though the K20/K and K20/H wells are very close to each other (Figure 1c). On the other hand, the coal-bearing Alacaağzı, Kozlu and Karadon formations in the K20/H well were identified between 1891.00–2002.20 m, 715.30–1891.00 m, and 424.70–715.30 m beneath the surface, respectively (Figure 1c). These are, as follows in the K20/K well: 1119.90–1251.61 m, 793.05–1119.90 m, and 468.70–793.05 m (Figure 1c).

During the Hercynian orogeny, the basin was uplifted and eroded; in turn, Permian sequences are mainly composed of reddish clastics (Kerey, 1985; Yalçın et al., 2002; Karayiğit et al., 2018a). Furthermore, post-Carboniferous cover formations consist of mainly Mesozoic sediments and volcanic rocks and Cenozoic units in the basin (Kerey, 1985; Tüysüz, 1999; Yalçın et al., 2002; Tüysüz et al., 2016). In both studied wells, the Late Jurassic (?) - Early Cretaceous Zonguldak Formation were the only cored cover formations (Figures 1c). The Aptian Kapuz limestone member in well K20/K was identified at 0–203.00 m depth, the lower Aptian İncivez clastic member cored at 203.00–264.55 m, and the Öküşne

limestone member was cut at 264.55–468.70 m beneath the surface, whereas Öküşne limestone and clastic members in well K20/H were determined between 0–287.00 m and 287.00–424.70 m beneath the surface, respectively (Figure 1c). The andesitic dykes in the basin are also reported in the post-Carboniferous cover formations, which locally caused thermally heated bituminous coals in the Gelik coalfield (Karayiğit, 1992).

3. Materials and methods

A total of eighty-one samples were taken from the K20/K and K20/H exploration wells in the Kozlu coalfield (Tables 1 and 2). The samples taken from the Zonguldak Formation are represented by clayey limestone, reddish marl, mudstone, and claystone layers. The samples from the Karadon and Kozlu formations are mostly composed of claystone and siltstone layers. Furthermore, tonstein (schieferton) layers were also observed in these formations. Finally, Alacaağzı Formation samples are mainly black claystone layers. Sample preparation was conducted in the laboratories of Hacettepe University, Department of Geological Engineering. The samples were crashed to less than 2 cm and ground in the disk mill for the X-ray diffraction analyses. The mineralogical composition of the raw samples, collected from drill-cores, was determined by Rigaku D/MAX 2200 PC XRD equipment. The equipment has CuKα radiation with a tube voltage and current of 40 kV and 30 mA, and a scanning speed of 2°/min from 2° to 70° 2θ at Hacettepe University (Ankara). The mineralogical compositions of whole-rock samples were determined using Rietveld based TOPAS-3 software. The results are calculated semiquantitatively following the methodology, as described by Oskay et al. (2016) in detail.

For detailed information about clay minerals, XRD clay fraction (XRD-CF) analysis was carried out on all studied samples. The clay fraction (<2-μm) was separated from the other components in the samples using the methods described in Temel and Gündoğdu (1996). The clay fraction separation was made by using sedimentation and centrifugation of the suspension after an overnight dispersion in distilled water. The clay particles were dispersed using ultrasonic vibration for approximately 15 min. In order to determine the clay minerals separated by the sedimentation method, the oriented specimens of the <2-μm fractions of each sample were prepared by air drying, ethylene-glycol solvation at 60 °C for 2 h, and thermal treatment at 490 °C for 2 h. The XRD-CF patterns were determined using Philips PW1140 XRD equipment. The mineral peak heights of the clay fraction diffractograms were measured, and semiquantitative percentages were calculated. Kaolinite was determined from its typical peak at 7–7.19 Å, absence of swelling with ethylene-glycol treatment, and peak collapse at 490 °C due to dehydroxylation. Chlorite was determined by a faint peak at 14.34 Å, an absence of swelling following ethylene-glycolation, and the maintenance of the reflection at 7–7.19 Å (reduced intensity) following heating at 490 °C. Characteristic peaks at 10–10.11 Å and 4.95–5.02 Å were used to determine illite/mica.

Prepared polished blocks of selected six whole-rock samples (K20/H-3, -15, -37 and -44, and K20/K-13 and -16) represented by Alacaağzı, Kozlu, Karadon, and Zonguldak formations were coated with carbon and were examined using with a Quanta 400 MK2 SEM, scanning electron microscope equipped with an EDAX Genesis XM4i energy dispersive X-ray spectrometer.

4. Results

The mineral compositions of the whole-rock and clay fraction of the samples taken from the Alacaağzı, Kozlu, Karadon, and Zonguldak formations are listed in Tables 1 and 2, while the selected XRD patterns are reported in Figures 2, 3, 4, and 5.

4.1. Mineralogical composition of Alacaağzı Formation

The samples from the Alacaağzı Formation are mainly composed of quartz, clay minerals, and feldspars (Tables 1 and 2). The clay minerals and quartz are abundant in this formation from both well profiles (Figures 6 and 7). Feldspar group minerals are relatively higher in some samples in the K20H well (Table 1). Pyrite, biotite, Ti-oxide, sphalerite, and iron oxides were observed as accessory phases during the SEM-EDX analyses. In addition, siderite overgrowths around pyrite grains are also observed (Figures 8 and 9). The Ca-Mn-bearing siderites and As-bearing pyrites were also observed during the SEM-EDX analyses (Figure 9). Kaolinite and illite/mica are dominant clay minerals in the Alacaağzı Formation according to XRD-CF data (Tables 1 and 2). Illite/mica displays higher proportions in the lower parts, while kaolinite becomes dominant in the upper part of the formation (Figures 6 and 7). The SEM-EDX analyses show that illite/mica grains consist of a generally measurable amount of Na, Cl, and Ti by SEM-EDX (Figures 8a–8d). Chlorite is also present in lesser amounts in the studied samples from the Alacaağzı Formation (Figures 6 and 7). Considering the mineralogical composition of coal seams within the formation (Karayiğit et al., 2018a), the samples in this study display similar clay mineral compositions.

4.2. Mineralogical composition of Kozlu Formation

The clay minerals and quartz are dominant in whole rock samples in this formation, whereas feldspars and calcite are detected in some samples in XRD traces (Tables 1 and 2). The tonstein (schieferton/brown claystone) sample (K20/H-25 990.30–990.50 m) in this formation is mainly composed of clay minerals and quartz, while illite/mica and kaolinite are detected in the XRD-CF (Table 1). In

Table 1. The mineralogical compositions of the K20/H samples identified by XRD in whole-rocks and clay-fractions.

Formation	Member	Age	Depth (m)		Sample No	Lithology	Whole-rock minerals %								Clay-fraction minerals %		
							Clay minerals	Quartz	Feldspar	Calcite	Dolomite	Ilmenite	Pyrite	Hematite	Chlorite	Illite/Mica	Kaolinite
Zonguldak	Ökülşne clastics	Early Barremian	289.15	289.25	1	Reddish mudstone	61	29		7				3	14	77	9
			313.00	314.00	2	Reddish mudstone	56	26		13	2			3	19	75	6
			330.50	331.50	3	Reddish mudstone	61	17	1	2	16			3	10	59	31
			360.95	361.05	4	Reddish mudstone	53	40	3					4	17	57	26
			396.50	397.50	5	Reddish claystone	62	29		5				4	19	62	19
			415.60	415.80	6	Reddish claystone	62	27		8				3	15	71	14
Karadon		Duckmantian-Asturian	425.00	425.20	7	Green claystone	78	20						2	17	52	31
			438.50	438.90	8	Green claystone	73	27							15	34	51
			453.05	438.9	9	Black claystone	73	25	2						17	20	63
			473.20	473.45	10	Gray claystone	85	13	1				1		3	14	83
			528.30	528.40	11	Black claystone	64	36							8	24	68
			565.80	565.90	12	Green claystone	73	23	4						24	31	45
			594.80	595.20	13	Green claystone	71	27	2						9	22	69
			625.00	625.30	14	Green claystone	72	28							11	28	61
			649.00	649.70	15	Green-black claystone	62	37	1						17	40	43
			672.10	672.80	16	Light gray claystone	75	24	1						15	32	53
Kozlu		Langsettian	715.80	716.30	17	Black claystone	67	33								23	77
			731.80	732.00	18	Light gray claystone	64	36							11	28	61
			756.30	756.60	19	Black claystone	64	36							12	41	47
			762.20	764.20	20	Black claystone	79	20	1						12	39	49
			871.50	871.60	21	Light gray claystone	69	29	2						12	36	52
			902.30	903.30	22	Dark gray claystone	81	19							6	14	80
			966.50	967.00	23	Black claystone	59	31	10						9	26	65
			973.20	973.35	24	Black claystone	77	23								22	78
			990.30	990.50	25	Brown claystone/Schifertone	80	20								33	67
			1032.00	1033.00	26	Black claystone	67	32	1						15	39	46
			1155.60	1156.10	27	Black claystone	80	20							14	57	29
			1207.70	1207.90	28	Black claystone	76	24							14	52	34
			1271.00	1271.30	29	Black claystone	64	30	6						13	41	46
			1367.20	1367.50	30	Black claystone	78	22							15	48	37
			1405.80	1405.90	31	Black claystone	75	20	5						17	43	40
			1476.80	1477.30	32	Black claystone	81	19							12	51	37
			1506.80	1507.00	33	Brownish sandstone	52	26	21	1					6	70	24
			1520.90	1521.00	34	Black claystone	72	19	9						9	65	26
			1557.30	1557.60	35	Black claystone	72	25	3						20	52	28
			1645.30	1645.60	36	Black claystone	70	30							12	60	28
			1675.30	1675.60	37	Black claystone	70	29		1					3	88	9
			1766.60	1766.80	38	Black claystone	80	20							12	62	26
Alacaağzı		Serpukhovian-Bashkirian	1891.25	1891.50	39	Black claystone	69	31							9	52	39
			1896.15	1896.25	40	Black claystone	54	44	2						6	28	66
			1907.25	1907.35	41	Black claystone	53	37	10						16	37	47
			1938.60	1938.80	42	Gray claystone	50	37	13						14	33	53
			1955.50	1955.60	43	Black claystone	70	30							19	43	38
			1988.00	1989.00	44	Black claystone	72	28							13	56	31

Table 2. The mineralogical compositions of the K20/K samples identified by XRD in whole-rocks and clay-fractions.

Formation	Member	Age	Depth (m)		Sample No	Lithology	Whole-rock minerals %								Clay-fraction minerals %			
							Clay minerals	Quartz	Plagioclase	Calcite	Dolomite	Ilmenite	Pyrite	Hematite	Chlorite	Illite/mica	Kaolinite	Illite/Smectite
Zonguldak	İncivez clastic	Early Aptian	220.70	220.80	1	Reddish marl	54	26	9	10				1	15	68	17	
			245.00	245.20	2	Reddish mudstone	62	35						3	4	58	38	
			258.00	259.00	3	Yellowish mudstone	53	46						1		57	43	
	Öküş. Lmst	Barre.	271.00	272.30	4	Reddish clayey limestone	83	11		6						93	7	
			342.00	343.50	5	Clayey limestone	48	25		21	3		3			100		
Karadon		Duckmantian-Asturian	469.00	469.70	6	Dark gray claystone	67	33								59	41	
			475.05	475.15	7	Gray claystone	63	35				2			2	30	68	
			476.65	476.75	8	Dark gray claystone	52	46				3			2	23	75	
			486.00	487.15	9	Dark gray claystone	72	28							9	41	50	
			498.35	500.00	10	Black siltstone	87	13							5	30	65	
			505.05	506.00	11	Black siltstone	70	30								25	75	
			523.75	525.00	12	Black siltstone	64	36							7	36	57	
			531.75	531.85	13	Black claystone/Schifertone?	100										100	
			555.00	555.45	14	Black claystone	89	10				1			9	42	49	
			557.00	557.25	15	Black claystone	80	20								28	49	23
			557.75	557.80	16	Brownish claystone /Schifertone?	76	23				2				15	72	13
			602.40	604.00	17	Black siltstone	69	29	1						14	32	54	
Kozlu		Langsettian	793.35	793.45	18	Black claystone	75	24	1						15	49	36	
			794.15	794.25	19	Black claystone	71	29							46	13	41	
			806.80	806.90	20	Gray claystone	77	22	11						12	56	32	
			863.75	863.80	21	Black claystone	63	28	10						15	48	37	
			877.70	877.90	22	Black sandy siltstone	63	26	11						13	48	39	
			893.50	893.80	23	Black claystone	75	24	1						13	51	36	
			918.45	918.60	24	Black claystone	78	22							13	68	19	
			934.80	935.10	25	Black claystone	74	21	5						11	40	49	
			951.65	951.80	26	Gray claystone	72	26	2						20	45	35	
			956.30	956.40	27	Black siltstone	63	29	8						16	45	39	
			974.90	975.00	28	Gray claystone	77	23							13	53	34	
			1051.20	1051.3	29	Gray siltstone	67	32	2						12	40	48	
			1086.70	1086.9	30	Black mudstone	56	33	10						13	42	45	
Alacaağzı		Serpukhovian-Bashkirian	1120.80	1121.00	31	Black claystone	83	17							6	24	70	
			1129.00	1129.65	32	Black claystone	57	33	10						17	35	48	
			1139.20	1139.30	33	Black claystone	72	26	3						15	39	46	
			1161.80	1161.95	34	Black claystone	58	32	10						11	41	48	
			1177.00	1177.35	35	Black claystone	70	26	4						14	44	42	
			1186.40	1187.00	36	Black claystone	75	24	1						6	67	27	
			1246.00	1246.50	37	Black claystone	56	34	10						12	52	36	

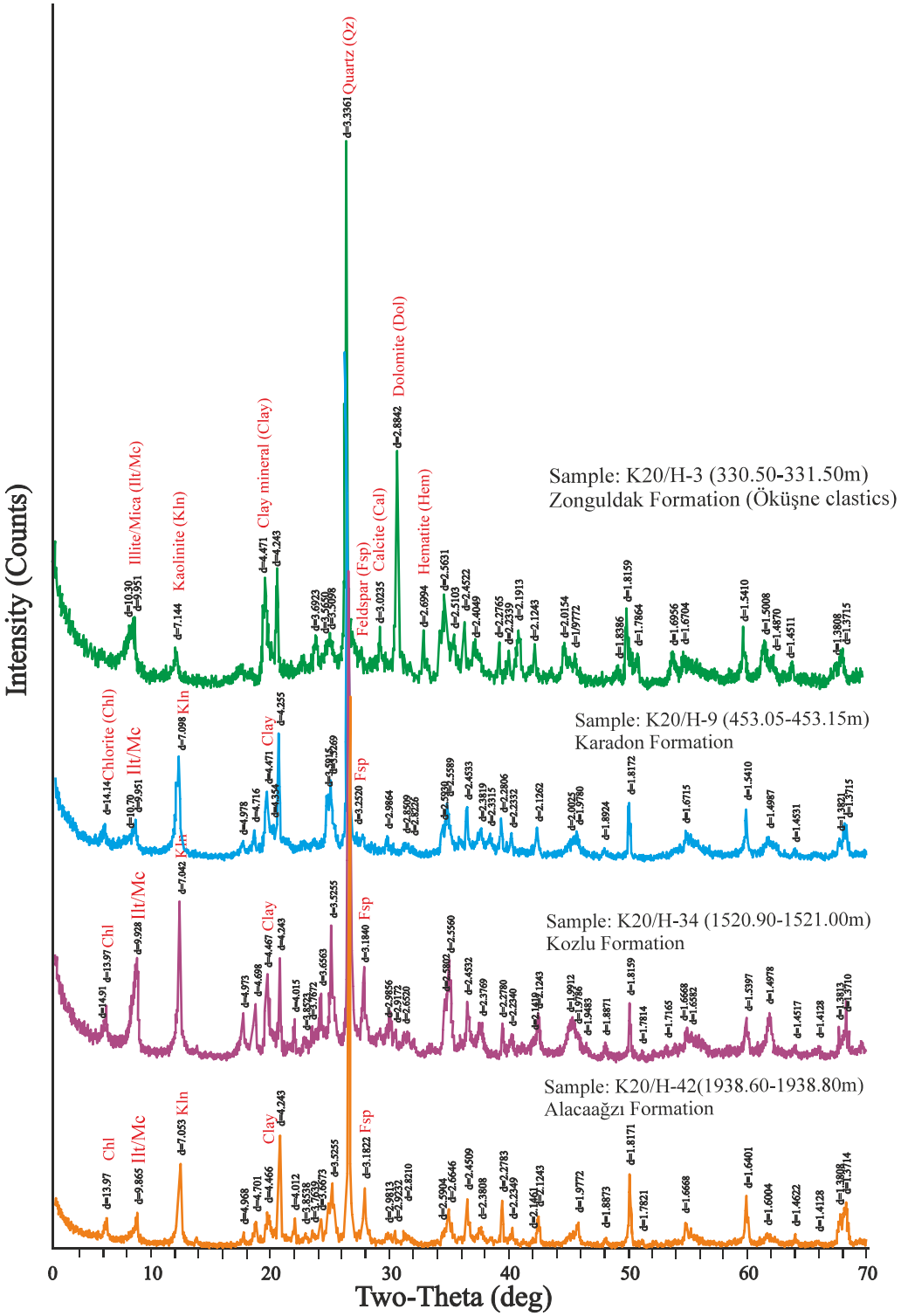

Figure 2. Selected XRD traces of whole-rock samples.

addition, F-Cl apatite (Figure 10a), Ti-bearing biotite and illite/mica (Figures 10a–10b and 11a–11d) and Sr-bearing phosphates (presumably goyazite) (Figures 10c–10d) were detected during the SEM-EDX analyses. Quartz and clay minerals display generally similar vertical distributions in the studied wells (Figures 6 and 7). Nevertheless, the vertical distributions of clay minerals in the XRD-CF traces show some differences in the K20/H and K20/K

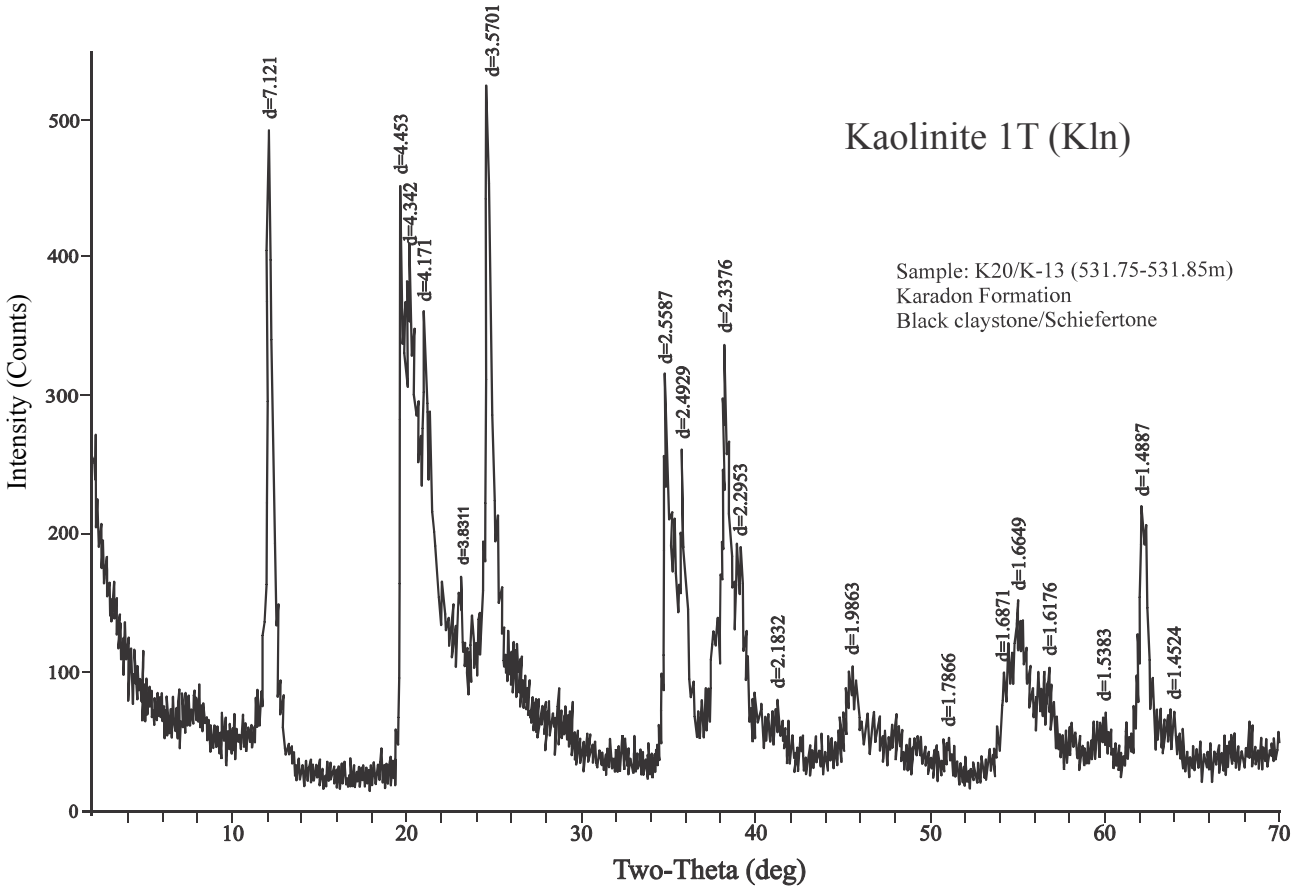

Figure 3. Whole-rock XRD trace of tonstein (schifertone) sample (K20/K-13).

well samples (Figures 6 and 7). Illite/mica and kaolinite are common clay minerals in the K20/H well samples. The samples from the Kozlu Formation in the K20/K well have relatively lower kaolinite proportions and relatively higher illite/mica proportions than their counterparts in the K20/H well (Tables 1 and 2). Illite/mica displays a decreasing trend towards the upper parts of the Kozlu Formation in the K20/H well, while kaolinite shows an increasing trend towards the upper part of the formation in this well (Figure 6). On the other hand, the vertical distributions of kaolinite and illite/mica in the K20/K well have not changed significantly in this formation (Figure 7). The vertical distributions of chlorite content in both display similar trends, except for the sample K20/K-19, in this formation (Figures 6 and 7). The similar mineralogical compositions of coal seams and the studied samples from the Kozlu Formation in this study could suggest that the redox conditions and origins of clastic influx into the deposition environment could be similar.

4.3. Mineralogical composition of Karadon Formation

Quartz and especially clay minerals are more common in whole rock samples from the Karadon Formation from both wells (Tables 1 and 2). In addition, feldspars, pyrite, and ilmenite are identified in the XRD traces of some samples from this formation (Tables 1 and 2). During the SEM-EDX analysis, Cl-F apatite, illite/mica, and biotite, partially altered to kaolinite, were frequently detected, while in some samples, siderite nodules were also detected (Figure 12). Of note, the presence of measurable Ti, Fe, and K from kaolinite by SEM-EDX (Figure 12d) could be related to the nano-biotite layers within kaolinite (Bauluz, 2013).

Tonstein (schieferton/claystone) samples (K20/K-13 (531.75–551.85 m) and K20/K-16 (557.75–557.80 m) were primarily made up of clay minerals (Table 2). The XRD whole-rock analysis of these samples shows that K20/K-13 is almost entirely composed of kaolinite, as in a typical tonstein (Figure 3), while kaolinite, quartz, and ilmenite were detected in sample K20/K-16 (Table 2). In XRD-CF analysis, the latter one includes kaolinite, illite/mica, and interstratified illite/smectite (I/S), presumably R1 and, to lesser extent, R3 (Table 2). Furthermore, ankerite, baddeleyite, barite, biotite, Cl-F apatite, calcite, U-bearing monazite, sphalerite, siderite, and Ti-oxides were also observed during the SEM-EDX analysis (Figures 13–15).

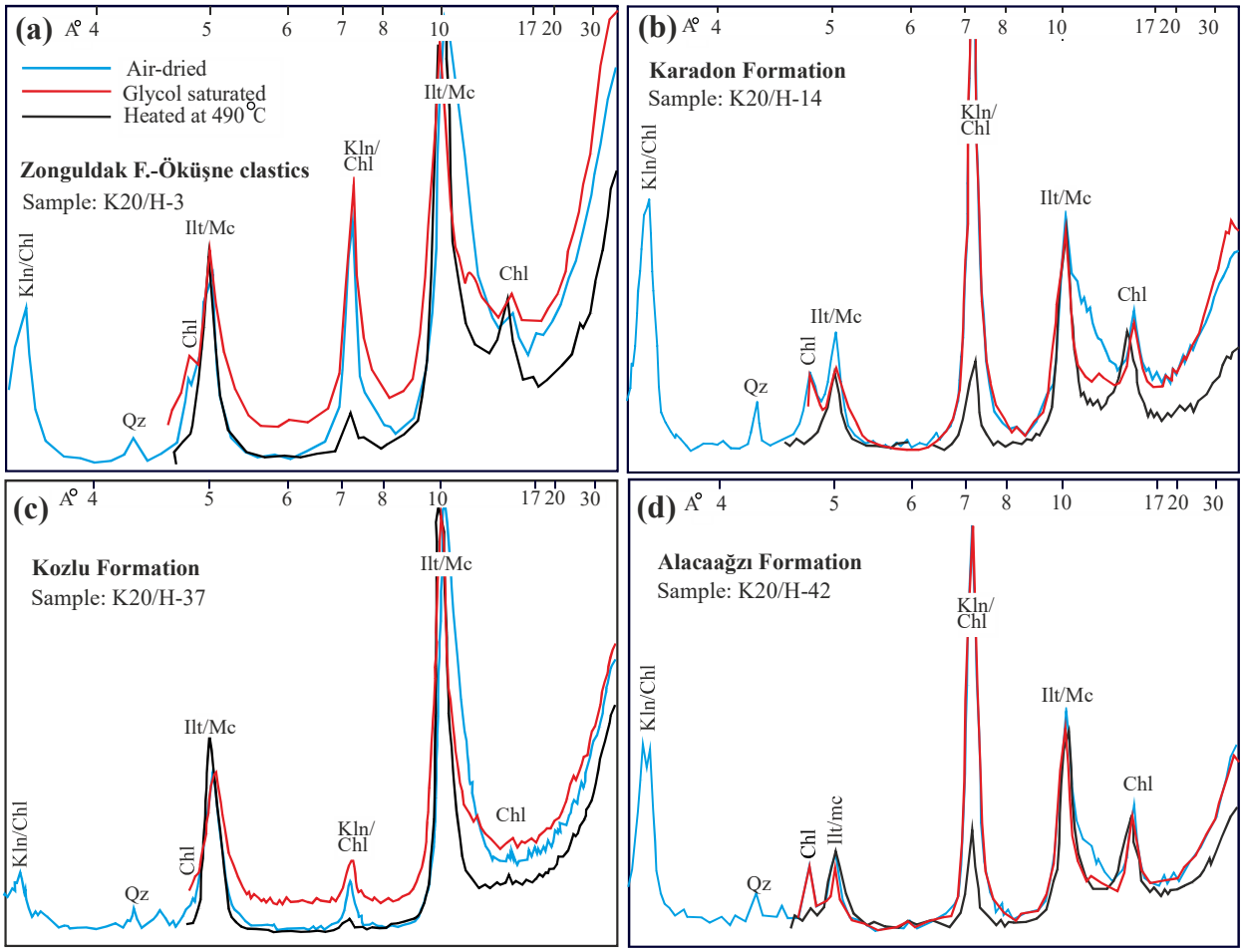

Figure 4. Selected X-ray diffractograms of the clay fractions of samples from the K20/H well (abbreviations: Chl: chlorite, Ilt/Mc: illite/mica, Kln: kaolinite, Qz: quartz).

The kaolinitic matrix in the tonstein layers hosts mainly apatite, quartz, feldspars, monazite, Ti-oxide, and zircon grains (Figures 13 and 14). Zircon grains are generally observed as well-preserved euhedral grains, while quartz and apatite grains generally display irregular shapes in the tonstein samples (Figures 13d and 15b). In addition, carbonate minerals (e.g., calcite and ankerite) and barite are observed within the cleat/fracture infillings of the studied samples (Figure 13e).

In the XRD-CF of this formation, kaolinite and illite/mica are more common, while chlorite displays lower proportions (Figures 6 and 7). In the K20/H well, kaolinite displays a decreasing trend towards the upper parts of the formation. In contrast, illite/mica shows an increasing trend in this well (Figure 6). In the K20/K well, the vertical distributions of kaolinite and illite/mica do not show clear increase or decrease trends throughout the formation; on the other hand, a relative negative trend between kaolinite and illite/mica could be pronounced in this well (Figure 7). The mineralogical compositions of coal seams cored in the K20/H and K20/K wells are similar to those of the Kozlu Formation; except pyrite as a minor phase in the coal seam (Karayiğit et al., 2018a).

4.4. Mineralogical composition of Zonguldak Formation

The samples of the Zonguldak Formation are mainly composed of clay minerals and quartz (Tables 1 and 2). Calcite and dolomite are the most common phases found in clayey limestone and mudstone; hematite is also found as a minor phase in reddish-coloured mudstone and clayey limestone (Tables 1 and 2). This could also explain the reddish colour of these samples. In addition, feldspars are only detected in two samples from the K20/H well, while pyrite is identified in one sample from the K20K well from this formation (Tables 1 and 2). Ankerite, Ti-oxides, biotite, and Fe-oxide (presumably hematite) were also observed during the SEM-EDX analysis (Figure 16). The SEM-EDX data also implies that dolomite and calcite grains contain a measurable amount of Fe in the Zonguldak Formation (Figure 16).

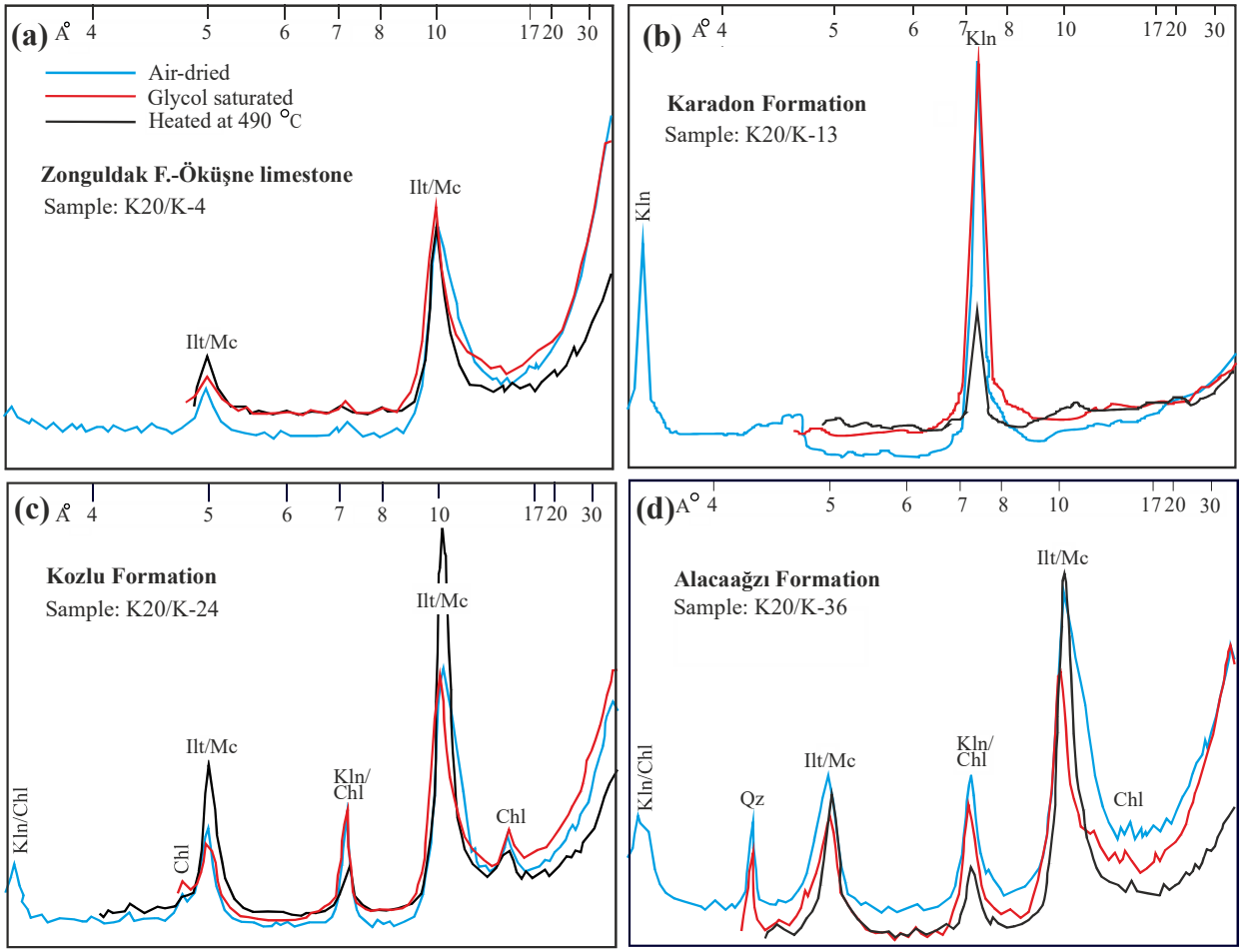

Figure 5. Selected X-ray diffractograms of the clay fractions of samples from the K20/K well (abbreviations: Chl: chlorite, Ilt/Mc: illite/mica, Kln: kaolinite, Qz: quartz).

The XRD-CF data shows that illite/mica, chlorite, and kaolinite are the identified clay minerals in the samples from the Zonguldak Formation (Figures 4, 5, 6, and 7). Illite/mica is abundant mineral in the Zonguldak Formation, while kaolinite displays relatively higher proportions than chlorite (Figures 6 and 7). Even though illite/mica is the predominant mineral in this formation cored in both wells, it has different vertical distributions throughout the formation. In the K20/K well, illite/mica displays a decreasing trend towards the upper parts of the formation in the K20/H well, while it has an increasing trend towards the upper parts (Figures 6 and 7). Furthermore, kaolinite displays relatively higher proportions in the central parts of the formation whereas the kaolinite proportions are generally low in claystone samples.

5. Discussion

The results of whole-rock XRD analysis of Late Carboniferous and Early Cretaceous formations sampled from clayey sedimentary rocks show that clay minerals are the predominant phases in both wells (Figures 6 and 7). Quartz is also another dominant phase in all studied formations from both wells, and it displays relatively higher proportions in samples from the Alacaağzı Formation in the K20/H well (Figure 6).

The proportion of quartz varies throughout the studied wells (Figures 6 and 7), and it is mostly observed as individual grains within the illitic matrix and as well as within the kaolinitic matrix, especially in tonstein samples (Figures 8a, 12a–12b, 13d, 14b, and 16b). The occurrence of individual grains within an illitic matrix could imply a detrital origin for quartz, while quartz/silica grains within a kaolinitic matrix in tonstein samples have a volcanogenic origin. Furthermore, cleat/fracture quartz/silica-infillings in the studied samples could be epigenetic in origin.

The vertical variations of clay minerals (illite/mica, chlorite, and kaolinite) using XRD-CF through the well profiles could be related to the depositional environmental changes and/or climate conditions during the Late Carboniferous and Late Cretaceous in the Zonguldak

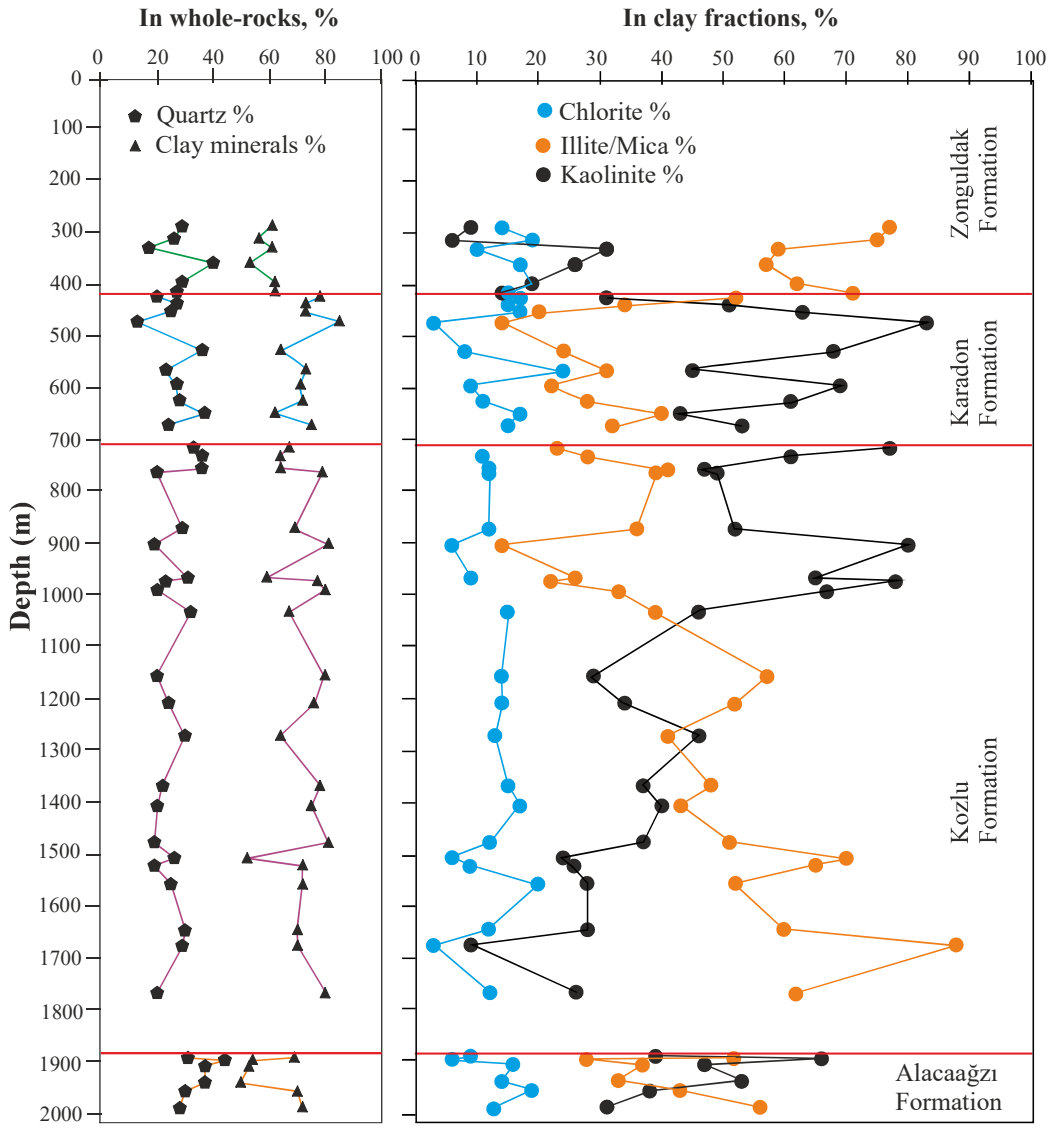

Figure 6. The vertical variations of quartz and clay minerals according to whole-rock XRD and chlorite, illite and kaolinite according to XRD-clay fraction in the K20/H well.

Basin. The main clay mineral of the Late Carboniferous sequences deposited in the lacustrine and meandering river environments is kaolinite which could suggest a wet climate condition; on the other hand, illite and chlorite are common clay minerals in the claystone samples that alternate with coarse-grained clastic deposited primarily in the braided river environment and/or arid climate conditions during the Late Carboniferous (Curtis, 1985; Deepthy and Balakrishnan, 2005; Erkoyun et al., 2019; Corentin et al., 2020). The previous palynological and paleobotanical studies show that wet and temperate climate conditions were common during the entire Late Carboniferous in the Zonguldak Basin (Akgün and Akyol, 1992; Cleal and van Waveren, 2012; Opluštil et al., 2018). Therefore, climatic influence on clay mineral formation during the Late Carboniferous seems to be very limited. The presence of reddish coloured mudstones and Fe-oxides in the Zonguldak Formation, on the other hand, might indicate that kaolinite was formed as a by-product of weathered illite/mica and/or biotite under hot and humid climate conditions (Deepthy and Balakrishnan, 2005; Kovács et al., 2013). As noted earlier, kaolinite is the main clay mineral in tonstein layers within the coal seams of the Kozlu and Karadon formations and possible volcanogenic mineral grains (e.g., apatite, feldspars, monazite, and zircon) were observed within kaolinitic matrices in these layers (Burger et al., 2000; Karayiğit et al., 2018a). Similarly, U-bearing monazite, feldspars, F-Cl apatite, Sr-bearing monazite, altered biotite, and Ti-oxide grains were detected within kaolinitic matrices by SEM-EDX in the

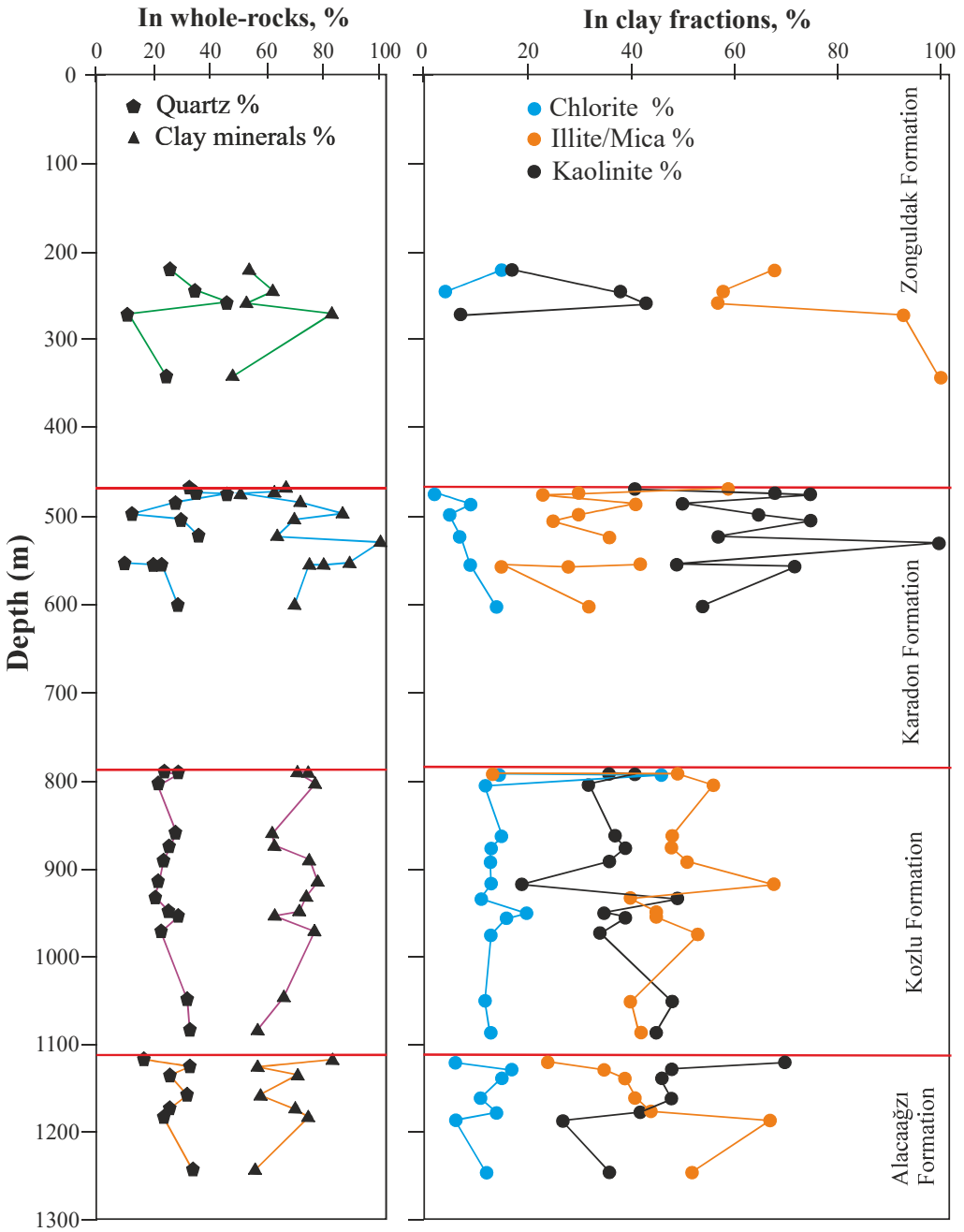

Figure 7. The vertical variations of quartz and clay minerals according to whole-rock XRD and chlorite, illite/mica and kaolinite according to XRD-clay fraction in the K20/K well.

studied sediment and tonstein samples (Figures 10–15), which indicate kaolinite in the Late Carboniferous samples are mainly derived from the alteration of volcanogenic clastic inputs in the depositional environment. The formation of such kaolinitic matrices in the coal-bearing sequences are generally related to the hydrogeological open system, where only Al and Si ions stayed into depositional environment (Bohor and Triplehorn, 1993; Ward and Gurba, 1999; Dai et al., 2015; Karayiğit et al., 2017; Erkoyun et al., 2019). Supporting this assumption, the existence of well-preserved euheudral zircon grains (Figure 15), and irregular quartz and apatite grains (Figures 13 and 14) within the kaolinitic matrix could also indicate a short-time interval tonstein formation and/or short distance transportation of pyroclastic material during the Late Carboniferous in the Zonguldak Basin (Arbuzov et al., 2016; Spears, 2012; Zhang et al., 2022). Furthermore, the existence of Ti-biotite (Figure 11a), and intergrowths

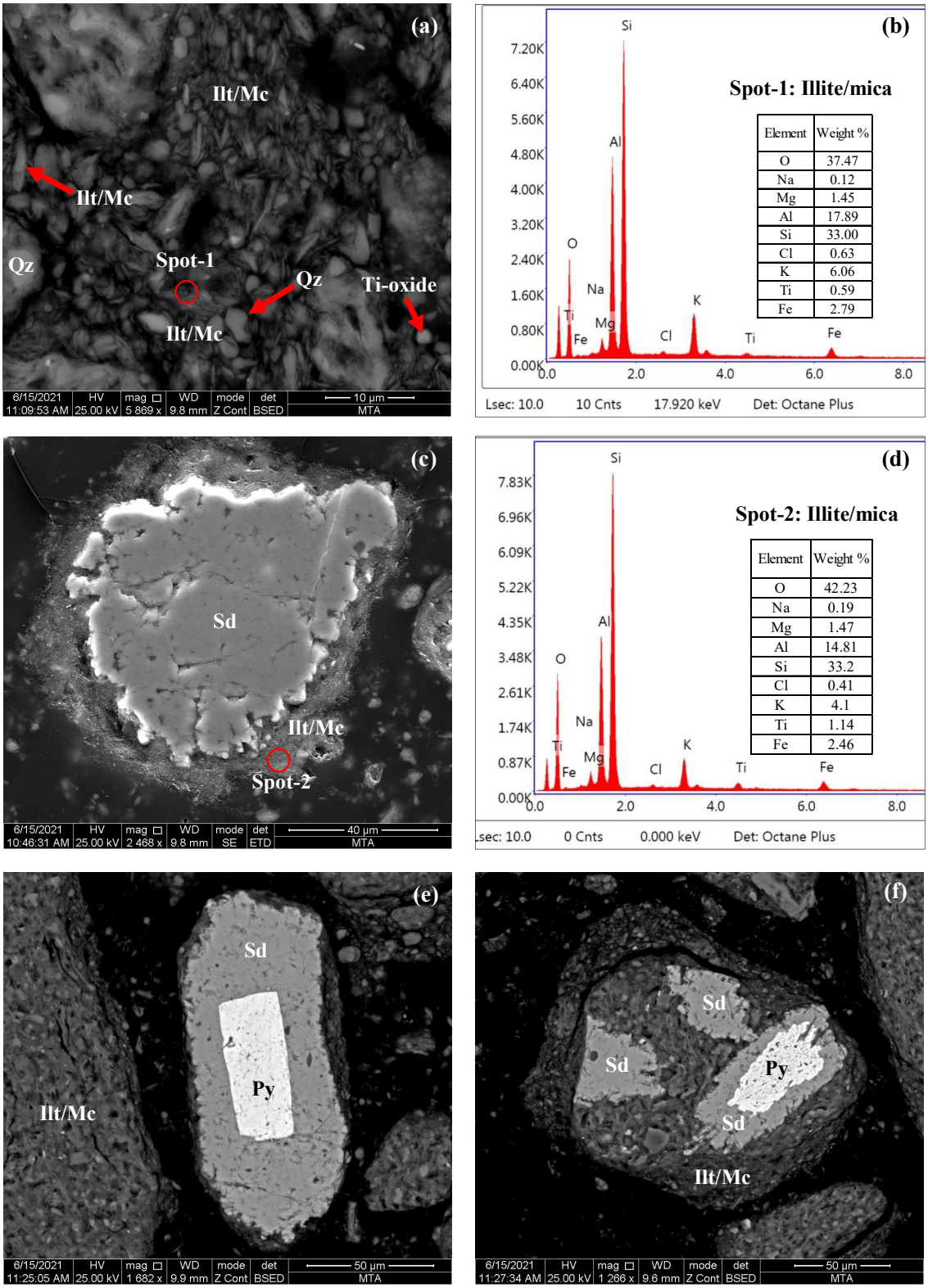

Figure 8. SEM backscattered (SEM-BSE) images of crystalline phases in the studied sample (K20/H-44) from the Alacaağzı Formation. (a) quartz (Qz) and Ti-oxide associated with illite/mica (Ilt/Mc); (b) EDX spectra of spot-1; (c) siderite (Sd) grain within illite/mica (Ilt/Mc); (d) EDX spectra of spot-2; (e) siderite (Sd) overgrowth around pyrite (Py) grain; (f) siderite (Sd) and pyrite (Py) grains within illite/mica (Ilt/Mc).

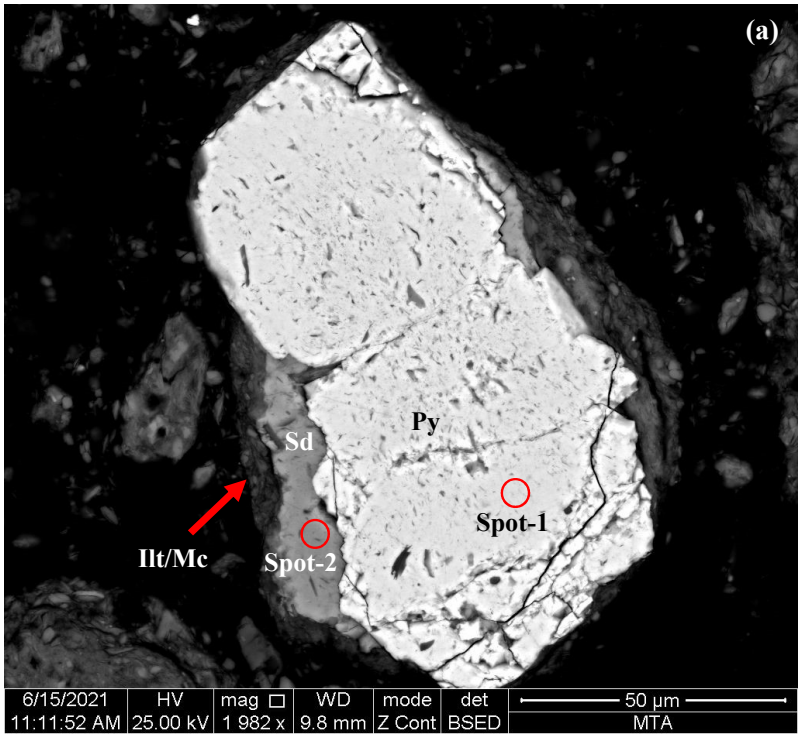

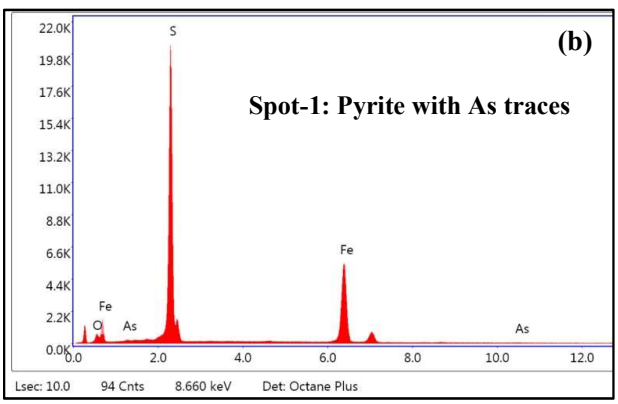

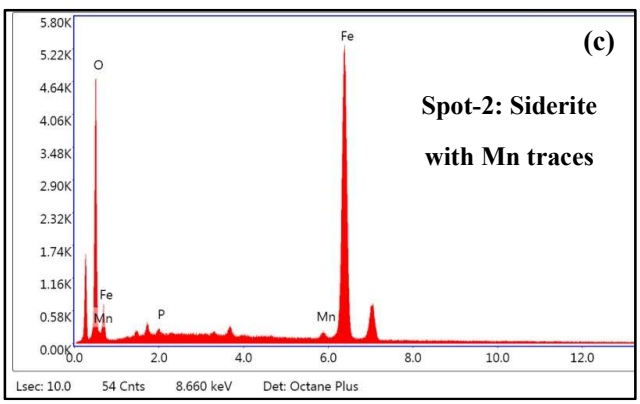

Figure 9. SEM-BSE images of crystalline phases in the studied sample (K20/H-44) from the Alacaağzı Formation. (a) siderite (Sd) overgrowth around pyrite (Py), and illite/mica (Ilt/mica); (b) EDX spectra of spot-1(As-bearing pyrite) in image a; (c) EDX spectra of spot-2 (Mn-bearing siderite) in image a.

between Ti-bearing biotite and kaolinite in the sediments (Figures 12c–12d) and tonstein samples of the Karadon and Kozlu formations could also suggest that kaolinite might also be derived from partial transformation of biotite to kaolinite within the depositional environment. In agreement, Ti-oxides within edge of kaolinite grains and layers between biotite grains (Figures 13c and 14c) might also be another indicator of alteration of biotite to kaolinite within the depositional environment. Nevertheless, the presence of cleat/fracture carbonate minerals (calcite and ankerite) and barite-infillings in the tonstein samples could be derived from precipitation of liberated Ca^{2+}, Mg^{2+} and Ba^{2+} ions leached solutions from the overlying Zonguldak Formation and/or the alteration of volcanogenic minerals (e.g., feldspars) (Bohor and Triplehorn, 1993; Burger et al., 2000; Çelik et al., 2021; Dai et al., 2015; Karayiğit et al., 2018a; Zhang et al., 2022).

In the studied samples, the majority of the illite/mica and biotite grains are probably of detrital origin in the studied formations, since the illitic matrix is associated with detrital mineral grains (Figures 8a–8b, 10c–10d, 11a–11c, 12a–12b, 13d, 14a, and 16). Such associations could indicate a high clastic influx derived from the adjacent areas, where pre-Carboniferous metamorphic

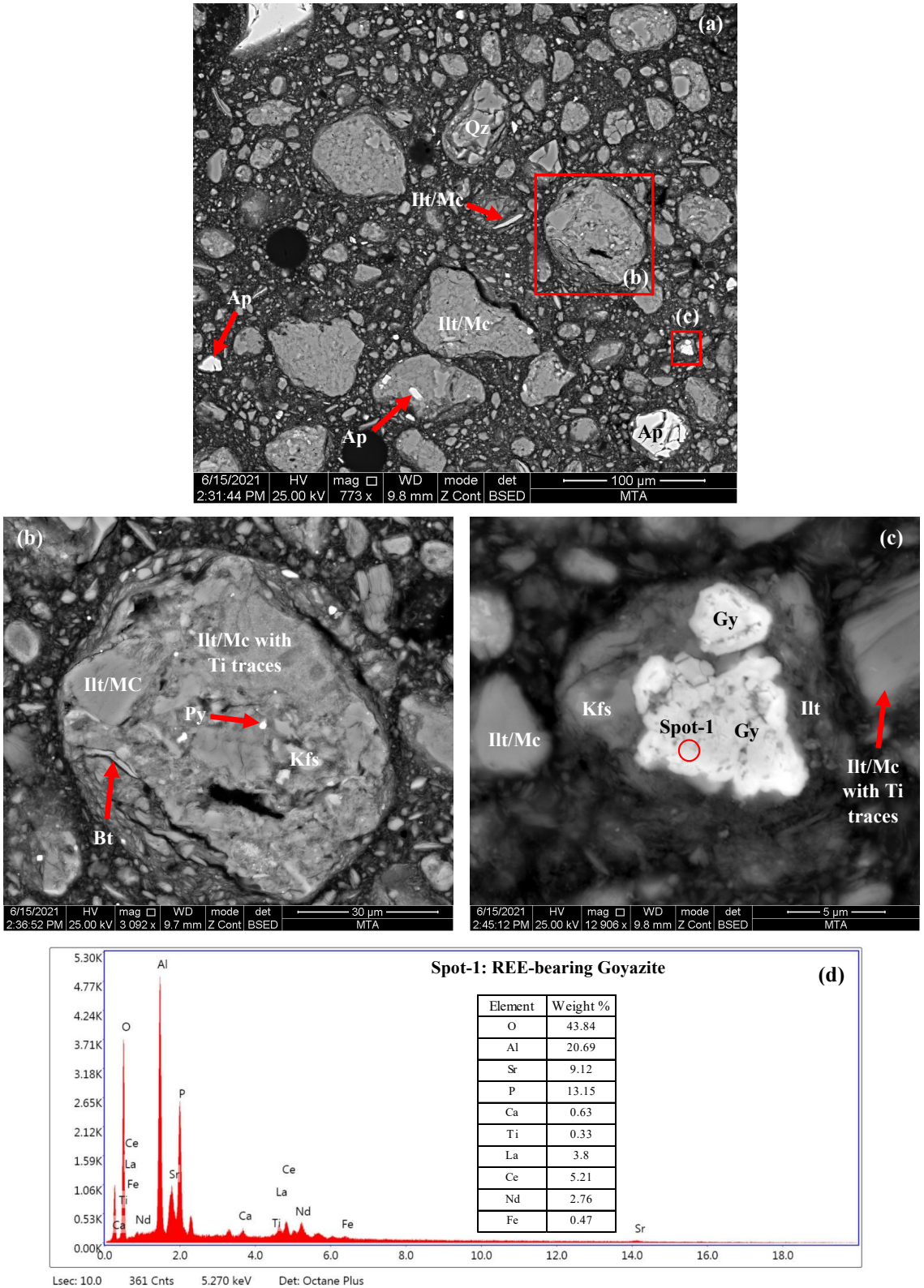

Figure 10. SEM-BSE images of crystalline phases in the studied sample (K20/H-37) from the Kozlu Formation. (a–c) apatite (Ap), biotite (Bt), goyazite (Gy), Kfs: K-feldspar, muscovite (Ms), and quartz (Qz) associated with illite/mica (Ilt/mica); (d) EDX spectra of spot-1 (rare earth elements (REE)-bearing goyazite) in image d.

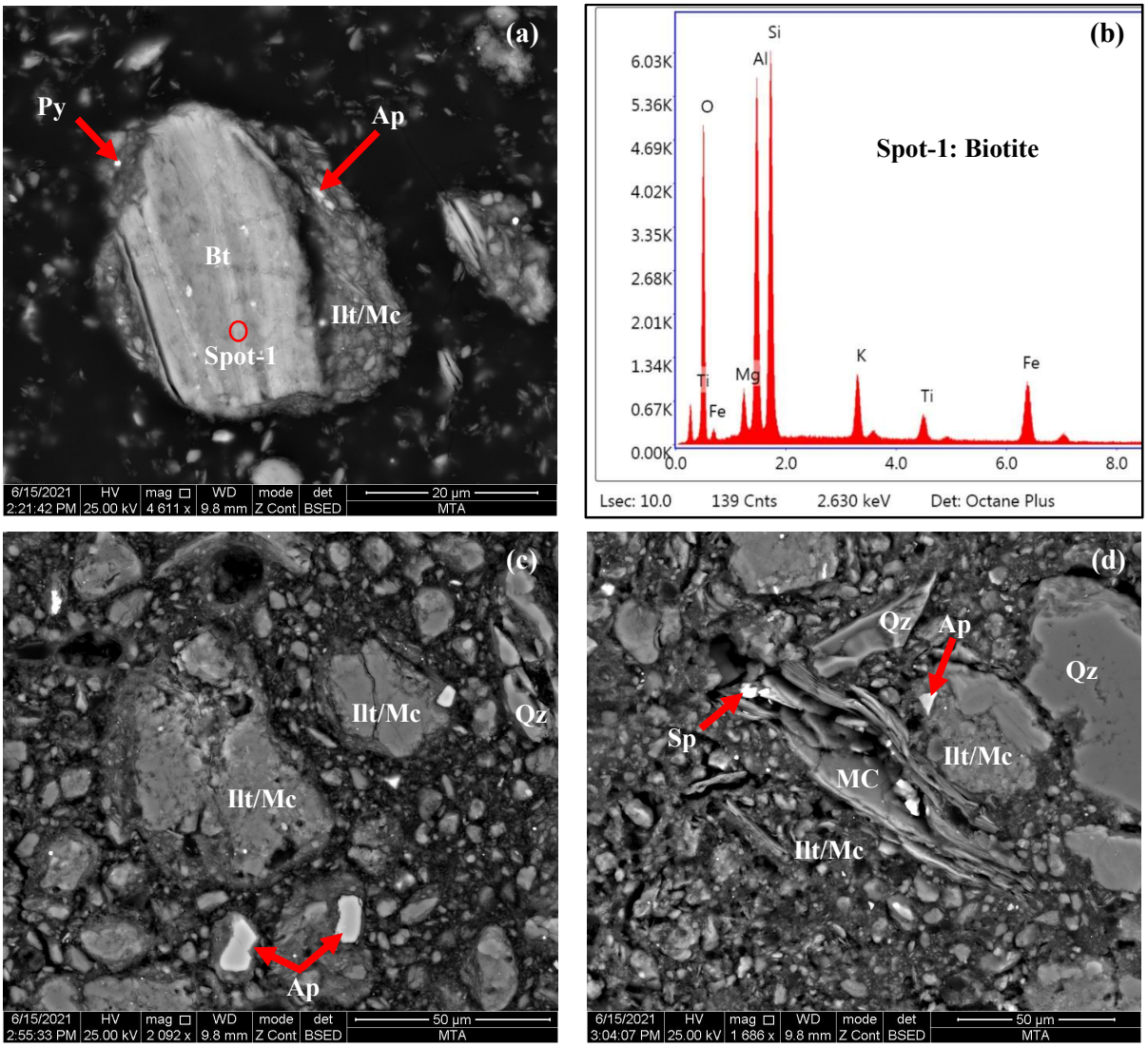

Figure 11. SEM-BSE images of crystalline phases in the studied sample (K20/H-37) from the Kozlu Formation. (a, c and d) apatite (Ap), biotite (Bt), muscovite (Ms), quartz (Qz) and sphalerite (Sp) associated with illite/mica (Ilt/mica); (b) EDX spectra of spot-1 (biotite) in image a.

and magmatic rocks are commonly outcropped. Bolstering this, the presence of muscovite, rounded quartz, and baddeleyite grains in the studied samples could also be an indicator of clastic inputs from the pre-Carboniferous basement rocks (Figures 8a, 11a, 12a, 13d, 15a). In contrast, Karayiğit (1991) stated that illite crystallinity of the Late Carboniferous sediment core samples from the coal exploration wells and floor and roof rocks of coal seams in the underground mines in the Zonguldak Basin suggest that illite mainly has a diagenetic origin, and, to a lesser extent, anchimetamorphism. The latter one might be related to clastic inputs from the pre-Carboniferous basement, which also explain the clastic illite/mica grains larger 2-µm in the recently studied wells, and the absence of correlations between previously reported vitrinite reflectance values and illite crystallinity by Karayiğit (1991). The discrepancy between illite crystallinity and vitrinite reflectance values also indicates illite/mica have detrital origin in the Zonguldak Basin, which also reported in Late Carboniferous very low metamorphized sediments in the USA (Kluth et al., 1981; Spötl et al., 1993; Verdal et al., 2011). The chemical compositions of illitic matrix in the samples might not indicate real mica chemistry according to mica nomenclature (Rieder et al., 1998); nevertheless, the presence of interstratified I/S in the Karadon Formation from the K20/K well (Table 2) could have originated from the transformation of smectite to interstratified I/S during the diagenesis (Curtis, 1985;

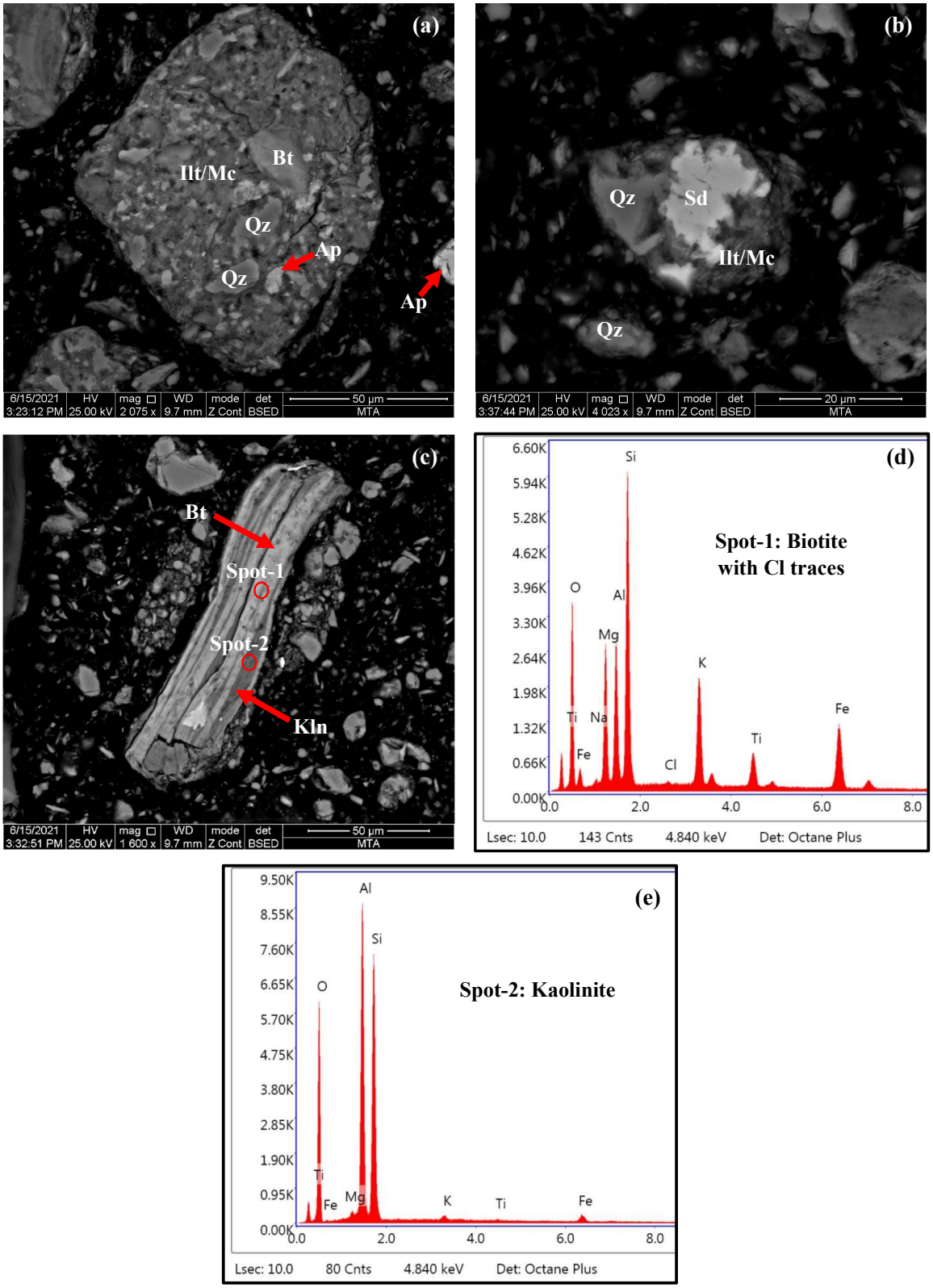

Figure 12. SEM-BSE images of crystalline phases in the studied sample (K20/H-15) from the Karadon Formation. (a–b) apatite (Ap), biotite (Bt), kaolinite (Kln), and quartz (Qz) associated with illite/mica (Ilt/Mc); (c) partially kaolinized biotite grain; (d) EDX spectra of spot-1 (Cl-bearing biotite) in image c; (d) EDX spectra of spot-2 (Ti-bearing kaolinite) in image c.

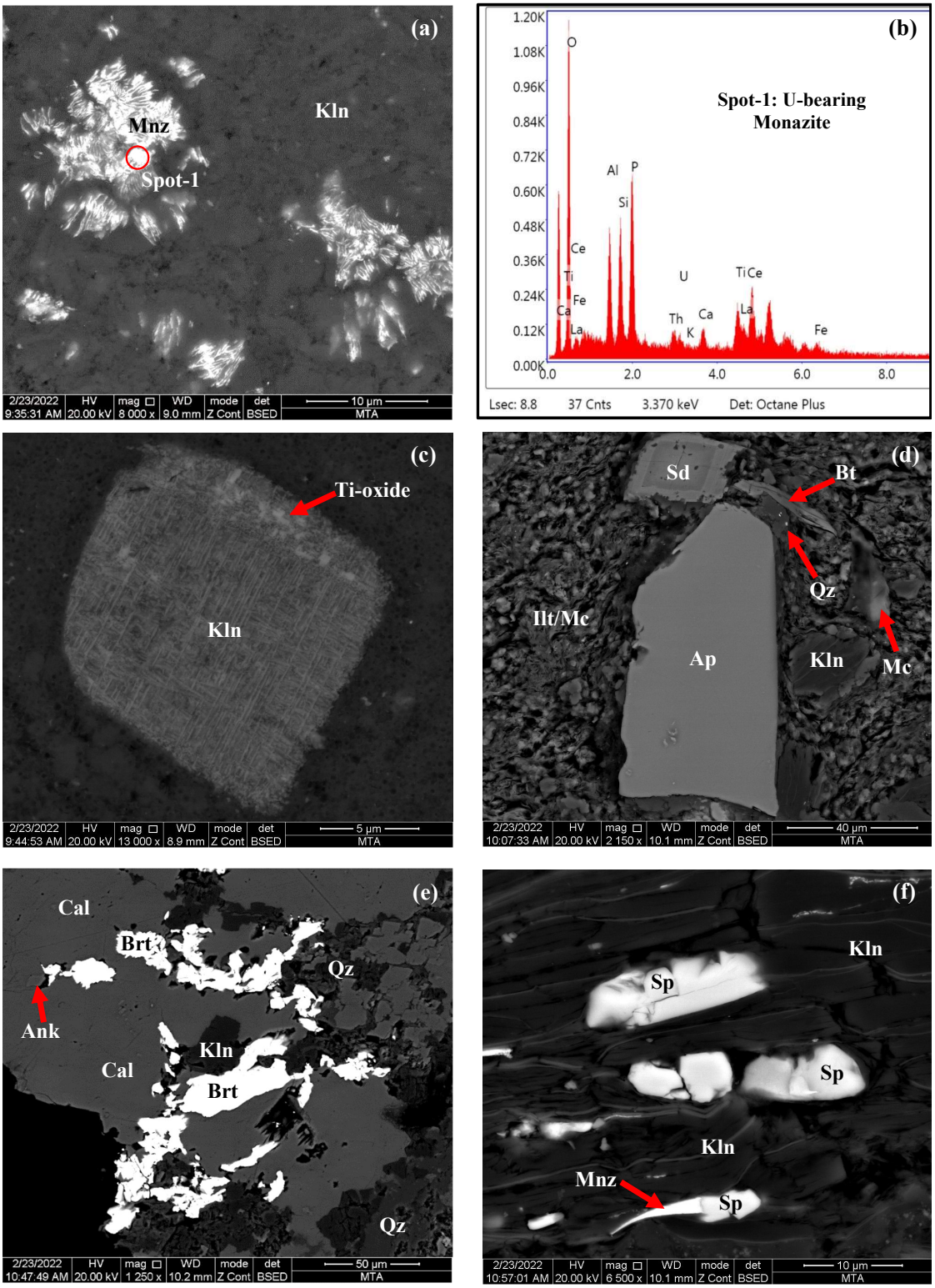

Figure 13. SEM-BSE images of crystalline phases in the studied tonstein (schifertone) samples (K20/K-13 (a–c) and K20/K-16 (d–f) from the Karadon Formation. (a, c, and f) sphalerite, U-bearing monazite (Mnz), sphalerite (Sp) and Ti-oxide associated with kaolinite (Kln); (b) EDX spectra of spot-1 (U-bearing monazite) in image a; (d) kaolinite (Kln), mica (Mc), siderite (Sd), quartz (Qz) and biotite (Bt) associated with illite/mica (Ilt/Mc); (e) quartz (Qz) associated with kaolinite (Kln) and cleat/fracture infilling ankerite (Ank), barite (Brt) and calcite (Cal).

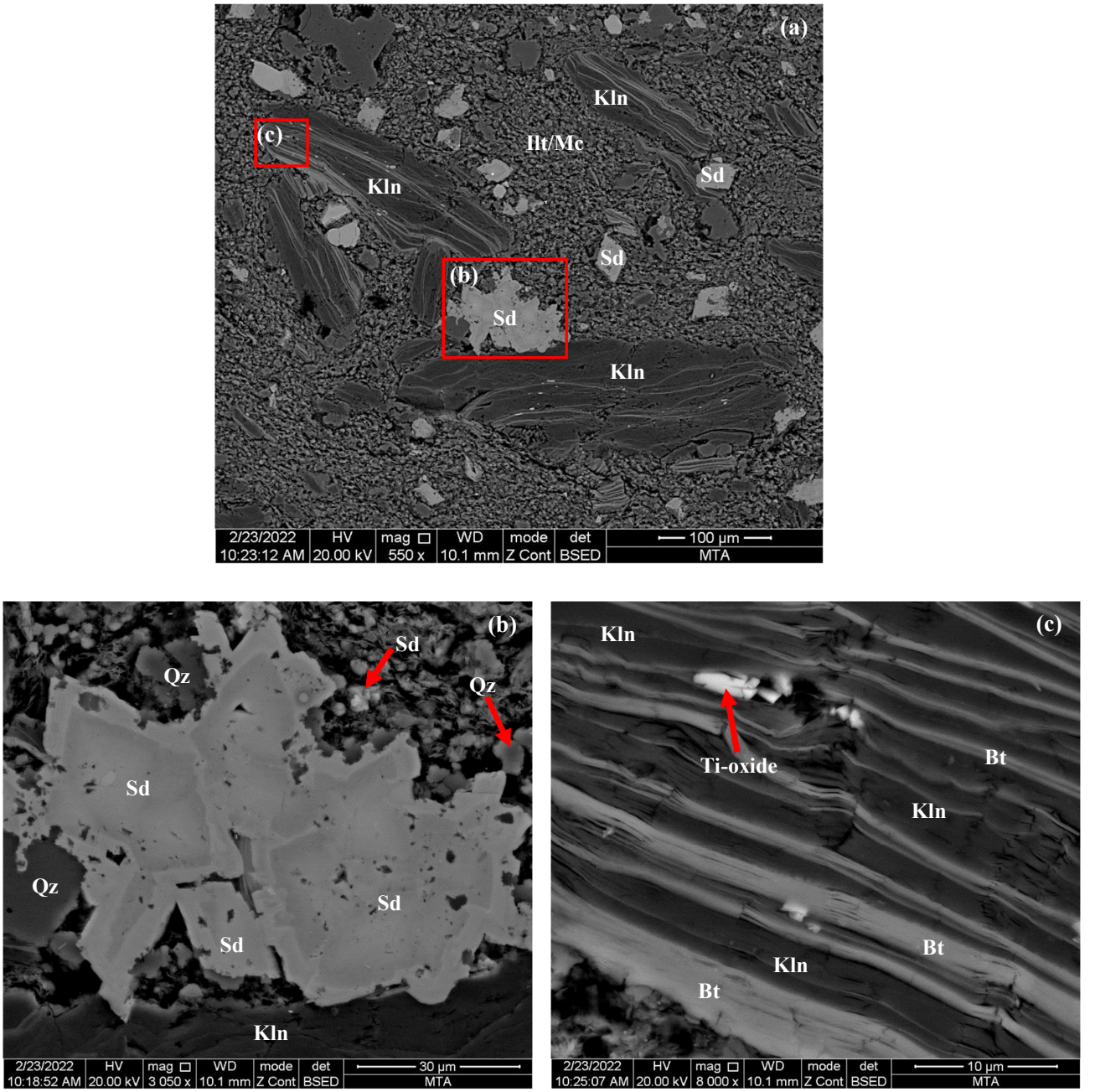

Figure 14. SEM-BSE images of crystalline phases in the studied tonstein (schifertone) sample (K20/K-16) from the Karadon Formation. (a) biotite (Bt), kaolinite (Kln) and siderite (Sd) nodules associated with illite/mica (Ilt/Mc); (b) detailed view of selected area in image a, quartz (Qz), siderite (Sd) nodules and kaolinite (Kln); (c) detailed view of selected area in image a, kaolinized biotite grain and Ti-oxides.

Lanson et al., 2009; Verdal et al., 2011; Wilson et al., 2016). For such smectite-I/S-illite (R1-R3) transition, burial depths could have been between 2400–3700 m with temperatures around 120–160 °C (Arostegui et al., 2006, 2019; Deon et al., 2022; Hower et al., 1976; Vrolijk, 1990). Even though the determination of certain burial depth of Late Carboniferous formation in the Zonguldak Basin could not be accurately estimated due to post-Mesozoic tectonic movements, the recent burial depth of the Late Carboniferous formations is between 425–1998 m in both wells, which is shallower than the necessary burial depth for the smectite-I/S-illite transition. The calculated T_{peak} temperatures using the random vitrinite reflectance of coal seams in the K20/K and K20/H wells are between

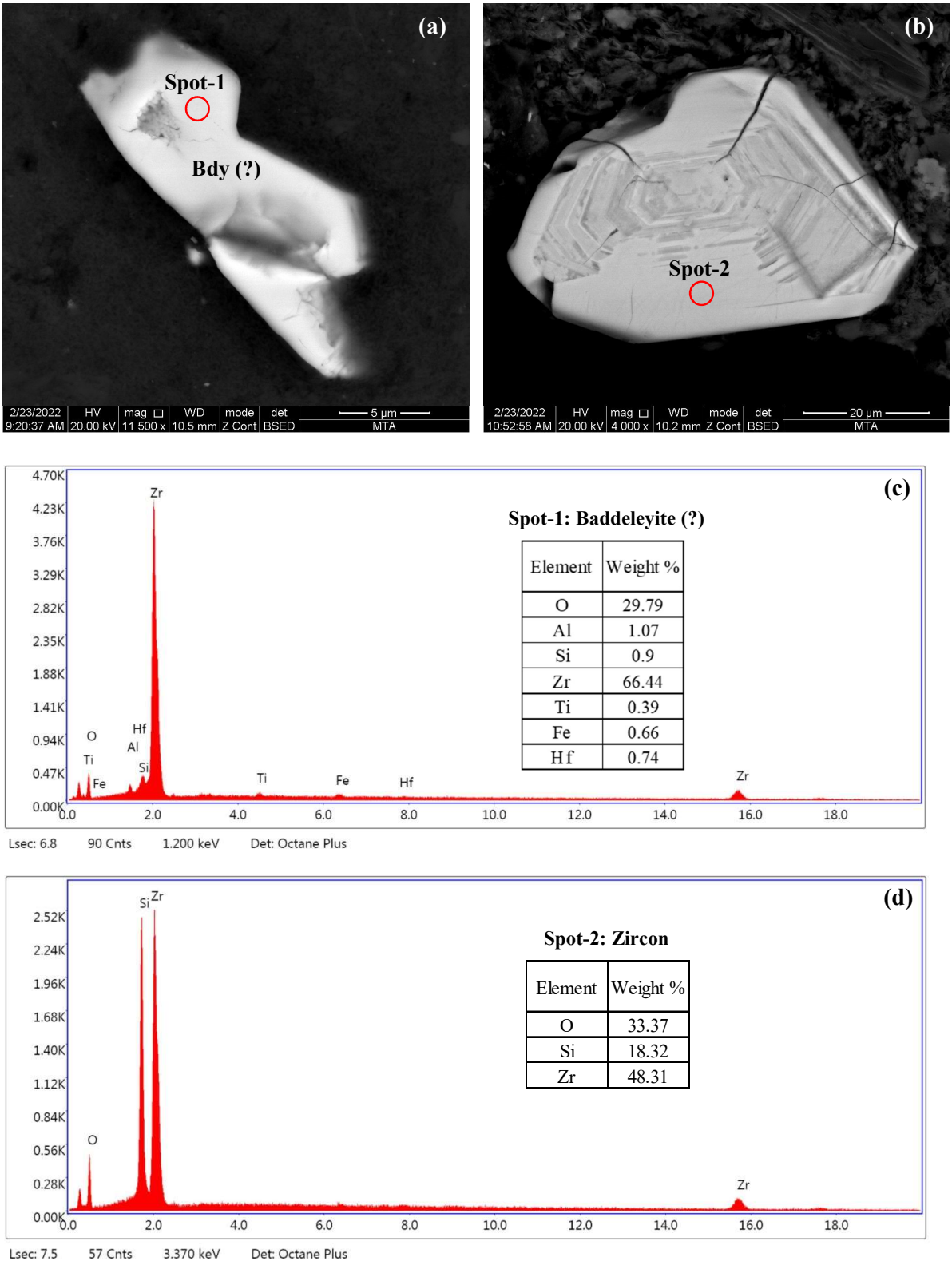

Figure 15. SEM-BSE images of crystalline phases in the studied tonstein (schifertone) sample (K20/K-13 (a) and K20/K-16 (b) from the Karadon Formation. (a) baddeleyite (Bdy) grain; (b) euhedral zircon grain; (c) EDX spectra of spot-1 (baddeleyite ?) in image a; (d) EDX spectra of spot-2 (zircon) in image b

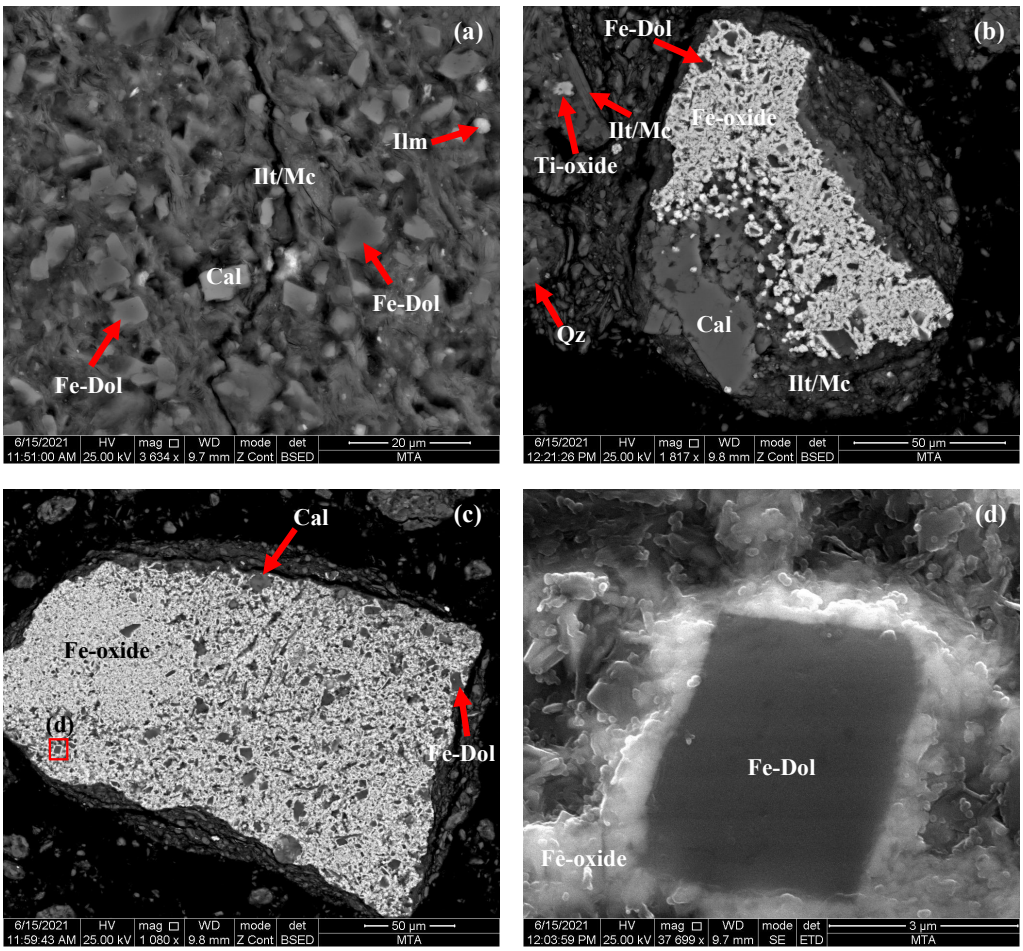

Figure 16. SEM-BSE (a–c) and secondary electrons (SE) images (d) of crystalline phases in the studied sample (K20/H-3) from the Zonguldak Formation. (a–b) calcite (Cal), ferroan-dolomite (Fe-Dol), Fe-oxide, quartz (Qz), and Ti-oxide associated with illite/Mc (Ilt/Mc), (c) calcite (Cal) and ferroan-dolomite (Fe-Dol) grains within Fe-oxide matrix; (d) detailed view of selected area in image c, ferroan-dolomite (Fe-Dol) grain within Fe-oxide matrix.

around 120–206 ± 30 °C (Karayiğit et al., 2018a). Hence, interstratified I/S in the Late Carboniferous formations also seems be to formed partially authigenically during the burial, and illitic matrix might be originated from transformation of detrital interstratified clay minerals or smectite during diagenesis. Furthermore, the T_{peak} temperatures and vitrinite reflectance are also in agreement with the lack of clear existence of R3 I/S interstratified clay mineral, which could be predominant around 240 °C, in the samples (Arostegui et al., 2006; 2019; Uysal et al., 2000). Nevertheless, detailed further studies using high resolution methods (e.g., TEM) for better understanding about chemical compositions of I/S matrix in the samples, especially K20K-15 and -16, should take place in future. The lower proportions of chlorite in the samples might be related to limited alteration of clastic biotite grains from pre-Carboniferous basement rocks or more possibly the by-products of biotite grains within the deposition environment.

Siderite is also identified as nodules in the Late Carboniferous samples in which illite and kaolinite generally display relatively higher proportions in the Late Carboniferous formations (Figures 8b–8d, 9a, 12b, and 14a–14b). Karayiğit et al. (2018a) also reported siderite nodules within a clay-mineral matrix and organic matter (macerals) in Late Carboniferous coal seams from the studied wells, which imply limnic and/or sulphate-deficient freshwater mire conditions (Karayiğit et al., 2017; Zhao et al., 2016). Besides, the presence of siderite nodules and the lack of pyrite grains in sediment samples in some Late Carboniferous samples could be an indicator of slightly higher alkaline conditions in the depositional environment

(Dai et al., 2020; Karayiğit et al., 2018a; Kortenski, 1992). The latter case might be more possible due to the presence of goyazite grains in the Late Carboniferous samples. Nevertheless, Ca-rich Mg siderite could be formed during peatification and/or early diagenetic stages after the formation of the kaolinite, likely as a result of the dissolution of volcanogenic mineral grains by the acidic waters in palaeomires (Thompson et al., 2019). Therefore, the liberated Ca, Fe, and Mg ions from the alteration of volcanogenic minerals (e.g., feldspars and biotite) within the depositional environment during the Late Carboniferous seem to have reacted with dissolved CO_2 in water, which could have originated from the decomposing plant matter. Furthermore, siderite overgrowths around pyrite grains in the Alacaağzı Formation could be related to the alternating Fe and sulphur concentrations and pH values of the depositional environment. This could also explain the presence of Fe-rich siderite overgrowths around CaMg-siderite nodules in the Karadon Formation (Figures 13d and 14b).

During the SEM-EDX analyses, iron-bearing dolomite and calcite were observed commonly in the Zonguldak Formation, which is mainly composed of limestone and clayey limestone. In addition, dolomite, calcite, and quartz minerals surrounded by an Fe-oxide matrix are also common in reddish mudstone and claystone samples from the Zonguldak Formation. In addition, the ferroan dolomite grains in the samples probably resulted from the penetration of Mg-Fe-bearing solutions into the carbonate rocks in the Zonguldak Basin from fault zones. Considering the reddish-colored limestones, Fe-oxides in this formation could also be an indicator for surface oxidation of short-term terrestrization and humid climate conditions during the Cretaceous or afterwards. Furthermore, macroscopically cleat/fracture carbonate-infillings were observed in some samples from the Kozlu Formation in the K20/H wells. The presence of cleats and fractures carbonate minerals infillings in coal seams could be developed from precipitation of Ca-Mg-Fe-rich solutions, during postcoalification, as noted earlier by Karayiğit et al. (2018a, 2018b). The source of such solutions could also be leached from Cretaceous-aged limestones.

6. Conclusions

The claystone layers cut by the K20/H and K20/K wells are mainly composed of quartz and clay group minerals. Feldspar, calcite, dolomite, siderite, and pyrite are present in lesser amounts. The clay group minerals are mainly represented by kaolinite, illite, and chlorite. The mineral abundances show differences related to the depositional environments. The majority of the illite/mica, chlorite, and kaolinite could be of detrital origin. However, some of the kaolinite minerals are probably derived from the alteration of the volcanic materials deposited synchronously with the Kozlu, Karadon, and Alacaağzı formations. In addition, interstratified I/S in the Late Carboniferous formations seems to be formed partially authigenically during the burial, and illitic matrix might be originated from transformation of detrital interstratified clay minerals or smectite during diagenesis. The distribution of the clay group minerals in the well profiles is generally related to the depositional environment and tectonic activity. Kaolinite is the main clay mineral of the claystones deposited in the lacustrine and meandering river environments during periods of effective low tectonic activity. The most common clay minerals of the claystones are illite/mica and chlorite, which alternate with coarse-grained clastics deposited in the braided river environment during intense tectonic activity. Quartz has a detrital origin and is observed in all samples. The feldspar content increases from the Karadon Formation towards the Alacaağzı Formation with depth. The presence of carbonate minerals in cleats and fractures could be related to the penetration of Mg-, Ca-, and Fe-rich solutions from cover formations into the coal-bearing sequences. On the other hand, Fe-oxide and siderite overgrowths surrounded calcite, dolomite, quartz, and pyrite minerals in the samples of Zonguldak and Alacaağzı formations, implying that the chemistry of water in the palaeomires was also changeable.

Acknowledgment

A part of this study was supported by the Turkish Scientific and Technological Research Council of Turkey (TÜBİTAK) under the project YDABCAG-70. The authors would like to thank Turkish Hard Coal Enterprises (TTK) for their providing core samples from wells, Drs. James HOWER (Kentucky University) and Rıza Görkem OSKAY (Hacettepe University) for their helps and suggestions during the manuscript preparation, and finally Dr. Tolga Görmüş and Mr. Ufuk Kibar (MTA) for their contributions during SEM study.

References

Ağralı B (1969). Palynological investigation and age determination of some coal seams from the Amasra Carboniferous Basin. Geological Bulletin of Turkey 12 (1-2): 10-28. (in Turkish with an abstract in French).

Akgün F, Akyol E (1992). Palynology and paleoecology of the coals in the Amasra-Bartın Carboniferous Basin. Turkish Journal of Earth Sciences 1: 49–56 (in Turkish with an abstract in English).

Arbuzov SI, Mezhibor AM, Spears DA, Ilenok SS, Shaldybin MV et al. (2016). Nature of tonsteins in the Azeisk deposit of the Irkutsk Coal Basin (Siberia, Russia). International Journal of Coal Geology 153: 99-111. https://doi:10.1016/j.coal.2015.12.001

Arostegui J, Arroyo X, Nieto F, Bauluz B (2019). Evolution of clays in Cretaceous Marly series (Álava block, Basque Cantabrian Basin, Spain): Diagenesis and detrital input control. Minerals 9: 40. https://doi:10.3390/min9010040

Arostegui J, Sangüesa FJ, Nieto F, Uriarte JA (2006). Thermal models and clay diagenesis in the Tertiary-Cretaceous sediments of the Alava block (Basque-Cantabrian basin, Spain). Clay Minerals 41: 791-809. https://doi:10.1180/0009855064140219

Bauluz B (2013). Clays in low-temperature environments. In: Nieto F, Livi KJT, and Oberti R (Eds.), Minerals at the nanoscale, Mineralogical Society of Great Britain and Ireland, London, pp. 181-216. https://doi:10.1180/EMU-notes.14.6

Bohor BF, Triplehorn DM (1993). Tonsteins: Altered volcanic-ash layers in coal-bearing sequences. Special Papers Geological Society of America 285: 1-44. https://doi:0813722853, 978-081372285-6

Burger K, Bandelow FK, Bieg G, (2000). Pyroclastic kaolin coal–tonsteins of the Upper Carboniferous of Zonguldak and Amasra, Turkey. International Journal of Coal Geology 45: 39–53. https://doi:10.1016/S0166-5162(00)00021-5

Canca N (1994). 1/100.000 scaled geological maps of western Black Sea hard coal basin (Turkey). MTA Publication, Ankara, Turkey: General Directorate of Mineral Research and Exploration (MTA) (in Turkish with an abstract in English).

Cleal CJ, van Waveren IM (2012). A reappraisal of the Carboniferous macrofloras of the Zonguldak-Amasra. Coal Basin, north-western Turkey. Geologia Croatica 65: 283–297. https://doi:10.4154/gc.2012.19

Curtis CD (1985). Clay mineral precipitation and transformation during burial diagenesis. Philosophical Transactions of the Royal Society A Mathematical Physical and Engineering Sciences 315: 91–105. https://doi:10.1098/rsta.1985.0031

Çelik Y, Karayiğit AI, Oskay RG, Kayseri-Özer MS, Christanis K et al. (2021). A multidisciplinary study and palaeoenvironmental interpretation of middle Miocene Keles lignite (Harmancık Basin, NW Turkey), with emphasis on syngenetic zeolite formation. International Journal of Coal Geology 237: 103691. https://doi:10.1016/j.coal.2021.103691

Corentin P, Deconinck J-F, Pellenard P, Amédro F, Bruneau L et al. (2020). Environmental and climatic controls of the clay mineralogy of Albian deposits in the Paris and Vocontian basins (France). Cretaceous Research 108: 104342. https://doi:10.1016/j.cretres.2019.104342

Dai S, Bechtel A, Eble CF, Flores RM, French D et al. (2020). Recognition of peat depositional environments in coal: A review. International Journal of Coal Geology 219: 103383. https://doi:10.1016/j.coal.2019.103383

Dai S, Li T, Jiang Y, Ward CR, Hower JC et al. (2015). Mineralogical and geochemical compositions of the Pennsylvanian coal in the Hailiushu Mine, Daqingshan Coalfield, Inner Mongolia, China: implications of sediment-source region and acid hydrothermal solutions. International Journal of Coal Geology 137: 92–110. https://doi:10.1016/j.coal.2014.11.010

Dean WT, Monod O, Rickards RB, Demir O, Bultynck P (2000). Lower Palaeozoic stratigraphy and palaeontology, Karadere-Zirze area, Pontus mountains, northern Turkey. Geological Magazine 137: 555–582. https://doi:10.1017/S0016756800004635

Deepthy R, Balakrishnan S (2005). Climatic control on clay mineral formation: Evidence from weathering profiles developed on either side of the Western Ghats. Journal of Earth System Sciences 114: 545-556. https://doi:10.1007/BF02702030

Deon F, van Ruitenbeek F, van der Werff H, van der Meijde M, Marcatelli C (2022). Detection of interlayered illite/smectite clay minerals with XRD, SEM analyses and reflectance spectroscopy. Sensors 22: 3602. https://doi:10.3390/s22093602

Erkoyun H, Kadir S, Huggett J (2019). Occurrence and genesis of tonsteins in the Miocene lignite, Tunçbilek Basin, Kütahya, western Turkey. International Journal of Coal Geology 202: 46-68. https://doi:10.1016/j.coal.2018.11.015

Gürdal G, Yalçın MN (2000). Gas adsorption capacity of Carboniferous coals in the Zonguldak Basin (NW Turkey) and its controlling factors. Fuel 79: 1913–1924. https://doi:10.1016/S0016-2361(00)00050-8

Hower J, Eslinger EV, Hower ME, Perry EA (1976). Mechanism of burial metamorphism of argillaceous sediment: 1. mineralogical and chemical evidence. Geological Society of America Bulletin 87: 725-737. https://doi:10.1130/0016-7606(1976)87<3C725:MOBMOA>3E2.0.CO;2

Karacan CÖ, Okandan E (2000). Fracture/cleat analysis of coals from Zonguldak Basin (northwestern Turkey) relative to the potential of coalbed methane production. International Journal of Coal Geology 44: 109–125. https://doi:10.1016/S0166-5162(00)00004-5

Karayiğit, Aİ (1991). Investigation of the variations of clay minerals and the illite crystallinite index of Kozlu and Karadon Formations in Zonguldak and Amasra Basin. Journal of Isparta Engineering Faculty of Akdeniz University, Geology Engineering Section I, 5: 133-147 (in Turkish with an abstract in English).

Karayiğit Aİ (1992). Linear relations among vitrinite reflections of coals in Zonguldak and Amasra basins. Turkish Journal of Earth Sciences 1: 43–48 (in Turkish with an abstract in English).

Karayiğit Aİ (2001). Mineralogy and trace element contents of the Akalin seam, Gelik mine, Zonguldak-Turkey. Energy Source 23: 699–709p. https://doi:10.1080/009083101316862453

Karayiğit Aİ (2003). Mineralogy and trace element contents of the Upper Carboniferous coals from the Asma-Dilaver and Gelik mines in Zonguldak, Turkey. Energy Source 25: 689–702. https://doi:10.1080/00908310390212417

Karayiğit Aİ, Gayer RA, Demirel İH (1998). Coal rank and petrography of Upper Carboniferous seams in the Amasra Coalfield, Turkey. International Journal of Coal Geology, 36: 277–294. https://doi:10.1016/S0166-5162(97)00047-5

Karayiğit Aİ, Littke R, Querol X, Jones T, Oskay RG et al. (2017). The Miocene coal seams in the Soma Basin (W. Turkey): insights from coal petrography, mineralogy and geochemistry. International Journal of Coal Geology 173: 110–128. https://doi:10.1016/j.coal.2017.03.004

Karayiğit Aİ, Mastalerz M, Oskay RG, Buzkan İ (2018b). Bituminous coal seams from underground mines in the Zonguldak Basin (NW Turkey): Insights from mineralogy, coal petrography, Rock-Eval pyrolysis, and meso-and microporosity. International Journal of Coal Geology 199: 91-112. https://doi:10.1016/j.coal.2018.09.020

Karayiğit Aİ, Mastalerz M, Oskay RG, Gayer RA (2018a). Coal petrography, mineralogy, elemental compositions and palaeoenvironmental interpretation of Late Carboniferous coal seams in three wells from the Kozlu coalfield (Zonguldak Basin, NW Turkey). International Journal of Coal Geology 187: 54-70. doi:10.1016/j.coal.2017.12.007

Kerey İE (1985). Facies and tectonic setting of the Upper Cretaceous rocks of northwestern Turkey. In: Dixon, J.E., Robertson, A.H.F. (Eds.), The Geological Evolution of the Eastern Mediterranean. Geological Society Special Publication 17: 123–128.

Kovács J, Raucsik B, Varga A, Újvári G, Varga G et al. (2013). Clay mineralogy of red clay deposits from the central Carpathian Basin (Hungary): Implications for Plio-Pleistocene chemical weathering and palaeoclimate. Turkish Journal of Earth Sciences 22: 414 – 426. https://doi:10.3906/yer-1201-4

Korstenski J (1992). Carbonate minerals in Bulgarian coals with different degrees of coalification. International Journal of Coal Geology 20 (3-4): 225-242. https://doi:10.1016/0166-5162(92)90015-O

Küskü O, Canca N, Hoşgörmez H, İnan S, Yalçın MN (1997). Geology. In: Yalçın MN (ed.), A multidisciplinary approach on Kozlu-K20/H and K20/K research wells. TÜBİTAK, Project number: YDABÇAG-70, Ankara, Turkey. pp. 4-19. (in Turkish with an abstract in English).

Kluth CF, Coney PJ (1981). Plate tectonics of the Ancestral Rocky Mountains. Geology 9: 10–15. https://doi:10.1130/0091-7613(1981)9<10:PTOTAR>2.0.CO;2

Lanson B, Sakharov BA, Claret F, Drits VA (2009). Diagenetic smectite-to-illite transition in clay-rich sediments: a reappraisal of X-ray diffraction results using the multi-specimen method. American Journal of Science 309: 476-516. https://doi:10.2475/06.2009.03

Okay AI, Nikishin, AM (2015). Tectonic evolution of the southern margin of Laurasia in the Black Sea region. International Geology Review 57 (5-8): 1051-1076. https://doi:10.1080/00206814.2015.1010609

Opluštil S, Lojka R, Pšenička J, Yilmaz Ç, Yilmaz M (2018). Sedimentology and stratigraphy of the Amasra coalfield (Pennsylvanian), NW Turkey – New insight from a 1 km thick section. International Journal of Coal Geology 195: 317-346. https://doi:10.1016/j.coal.2018.06.013

Oskay RG, Christanis K, Inaner, H, Salman, M, Taka, M (2016). Palaeoenvironmental reconstruction of the eastern part of the Karapınar-Ayrancı coal deposit (Central Turkey). International Journal of Coal Geology 163: 100-111. https://doi:10.1016/j.coal.2016.06.022

Rieder M, Cavazzini G, D'yakonov Yu-S, Frank-Kamenetskii VA, Gottardi G et al. (1998). Nomenclature of the micas. The Canadian Mineralogist 36: 905-912.

Spears DA (2012). The origin of tonsteins, an overview, and links with seatearths, fireclays and fragmental clay rocks. International Journal of Coal Geology 94: 22-31. https://doi:10.1016/j.coal.2011.09.008

Spötl C, Houseknecht DW, Jaques R (1993). Clay mineralogy and illite crystallinity of the Atoka Formation, Arkoma Basin, and frontal Ouachita Mountains. Clays and Clay Minerals 41: 745-754. https://doi:10.1346/CCMN.1993.0410614

Temel A, Gündoğdu MN (1996) Zeolite occurrences and the erionite-mesothelioma relationship in Cappadocia, central Anatolia. Mineralium Deposita 31: 539-547. https://doi:10.1007/BF00196134

Thompson LN, Finkelman RB, Arbuzov SI (2019). Water-rock interactions: The formation of an unusual mineral assemblage found in a Siberian coal. In: E3S Web of Conferences 98: 01050. https://doi:10.1051/e3sconf/20199801050

Tüysüz O (1999). Geology of the Cretaceous sedimentary basins of the Western Pontides. Geological Journal 34: 75–93. doi:10.1002/(SICI)1099-1034(199901/06)34:1/2<75:AID-GJ815>3.0.CO;2-S

Tüysüz O, Melinte-Dobrinescu MC, Yılmaz İÖ, Kirici S, Švabenická L et al. (2016). The Kapanboğazı formation: a key unit for understanding Late Cretaceous evolution of the Pontides, N Turkey. Palaeogeography, Palaeoclimatology, Palaeoecology 441: 565–581. https://doi:10.1016/j.palaeo.2015.06.028

Uysal IT, Glikson M, Golding SD, Audsley F (2000). The thermal history of the Bowen Basin, Queensland, Australia: vitrinite reflectance and clay mineralogy of late Permian Coal Measures. Tectonophysics 323: 105-129. https://doi:10.1016/S0040-1951(00)00098-6

Verdal C, Niemi N, van der Plujm BA (2011). Variations in the illite to muscovite transition related to metamorphic conditions and detrital muscovite content: insight from the Paleozoic passive margin of the southwestern United States. Journal of Geology, 119: 419-437. https://doi:10.1086/660086

Vrolijk P (1990). On the mechanical role of smectite in subduction zones. Geology, 18: 703–707. https://doi:10.1130/0091-7613(1990)018<0703:OTMROS>2.3.CO;2

Ward CR, Gurba LW (1999). Chemical composition of macerals in bituminous coals of the Gunnedah Basin, Australia, using electron microprobe techniques. International Journal of Coal Geology 39 (4): 279–300. https://doi:10.1016/S0166-5162(98)00049-4

Wilson MJ, Shaldybin, MV., Wilson, L (2016). Clay mineralogy and unconventional hydrocarbon shale reservoirs in the USA. I. Occurrence and interpretation of mixed-layer R3 ordered illite/smectite. Earth-Science Reviews 158: 31–50. https://doi:10.1016/j.earscirev.2016.04.004

Yalçın MN, Inan S, Gürdal G, Mann U, Schaefer RG (2002). Carboniferous coals of the Zonguldak Basin (northwest Turkey): implications for coalbed methane potential. AAPG Bull. 86: 1305–1328. doi:10.1306/61EEDC88-173E-11D7-8645000102C1865D

Yilmaz Y, Tüysüz O, Yiğitbaş E, Genç ŞC, Şengor AMC (1997). Geology and tectonic evolution of the Pontides. In: Robinson, A.G. (Ed.), Regional and Petroleum Geology of the Black Sea and Surrounding Region. AAPG Memoirs 68: 183–226.

Yürüm Y, Dilara B, Yalçın MN (2001). Change of the structure of coals from the Kozlu K20 G borehole of Zonguldak Basin with burial depth 1. Chemical structure. Energy Source 23: 511–520. doi:10.1080/00908310152125157

Zhao L, Sun J, Guo W, Wang P, Ji D (2016). Mineralogy of the Pennsylvanian coal seam in the Datanhao mine, Daqingshan Coalfield, Inner Mongolia, China: genetic implications for mineral matter in coal deposited in an intermontane basin. International Journal of Coal Geology 167: 201-214. https://doi:10.1016/j.coal.2016.10.006

Zhang Z, Dawei, Lv, Wang C, Hower JC, Raji M et al. (2022). Mineralogical and geochemical characteristics of tonsteins from the Middle Jurassic Yan'an Formation, Ordos Basin, North China. International Journal of Coal Geology 253: 103968. https://doi:10.1016/j.coal.2022.103968